# Unraveling the Peri-Implant Epithelial Barrier

*by*
Joseph Arthur Grauer

A thesis
presented to the University of Manitoba
in the fulfillment of the
requirements for the course DDSS 7220 Research Project

Winnipeg, Manitoba, Canada, 2024

## Examining Committee Membership

The following served on the Research Advisory Committee for this research project.

| | |
|---|---|
| Supervisor and External Examiner | Jill A. Helms<br>Professor, Stanford University |
| Co-Supervisor and Internal Member | Chrysi Stavropoulou<br>Assistant Professor, University of Manitoba |
| Internal Member | Anastasia Kelekis-Cholakis<br>Dean and Associate Professor, University of Manitoba |
| Chair of Oral Presentation | Raj Bhullar<br>Professor, University of Manitoba |

## Author's Declaration

I hereby declare that I am the sole author of this thesis. This is a true copy of the thesis, including any required final revisions, as accepted by my examiners.

I understand that my thesis may be made electronically available to the public.

## Abstract

The long-term success of dental implants relies on the formation of a protective soft tissue barrier that limits pathogen infiltration into peri-implant tissues. However, our understanding of how this barrier develops under different implant placement protocols (i.e., immediate vs. delayed placement) and in response to varying implant surface characteristics remains limited.

This study systematically evaluates the formation and maturation of peri-implant soft tissues in two contexts: (1) immediate versus delayed implant placement and (2) anodized versus machined implant surfaces.

Part I: Miniaturized titanium implants were placed in either fresh extraction sockets or healed maxillary first molar sites in mice. Peri-implant soft tissues were assessed at multiple time points to investigate molecular attachment mechanisms and the barrier function of the soft tissue. A healthy junctional epithelium served as a positive control. Notably, no significant differences were observed in the rate of soft tissue integration between immediate and delayed implants. However, mucosal integration took at least twice as long as osseointegration in this model.

Part II: Scanning electron microscopy and surface chemistry characterization were performed on miniaturized anodized and machined implants. Following placement in fresh extraction sockets, peri-implant tissues were examined at four time points. The findings corroborated those from Part I and led to several key conclusions:

1. Maturation of the peri-implant epithelium (PIE) is a prolonged process, aligning with clinical observations.
2. Soft tissue integration occurs more slowly than bone integration.
3. Anodized implant surfaces offer a transient advantage in promoting soft tissue maturation.

Together, these findings highlight the extended timeline required for PIE maturation, underscoring the potential clinical benefits of strategies aimed at accelerating this process.

## Acknowledgements

To begin, I would like to express my deepest gratitude to Professor Jill Helms, my primary advisor. She is a prolific researcher, a selfless and devoted mentor, and an avid horse rider and proud chief rancher at *Follow Your Bliss Farm*. She redefines the meaning of "*Minnesotan Nice*," consistently going above and beyond in her advisory and mentorship roles. I first reached out to her after my first year of D.M.D. studies, and she welcomed me into her lab with open arms (*literally!),* giving me the opportunity to explore the role of stem cells in the junctional epithelium. Joining her lab that summer felt like a stroke of incredible luck, and it has profoundly shaped my career aspirations. Prof. Helms has been instrumental in helping me navigate my decision to pursue a dental specialty and has provided invaluable insights every step of the way.

I am immensely grateful for her guidance throughout my research projects during my D.M.D. studies and for taking me on as a master's student. Her unwavering enthusiasm and support have been fundamental to my development as a researcher and my journey to becoming a periodontist. She has equipped me with the ability to thoughtfully develop new research questions and critically analyze existing literature. Through countless opportunities, Prof. Helms has given me the confidence to pursue my goals. I truly cannot thank her enough.

I also want to extend my sincere appreciation to Dr. Chrysi Stavropoulou, my internal supervisor, for her enthusiastic support of my project and for enabling me to explore my research passions through an international collaboration: an opportunity for which I will be forever grateful. Beyond her support for my research, she has guided me in developing my clinical skills and helped me bridge the gap between periodontal research and everyday clinical practice.

My heartfelt thanks also go to Dr. Anastasia Cholakis, my internal committee member and clinical mentor. Her invaluable insights into my project and research pursuits have drawn from a distinguished career in both academia and private practice. Beyond that, she has played a critical role in my development as a clinician, offering guidance and patience that have been essential to my growth, not just as a researcher, but also as a future periodontist.

Finally, I want to thank my family. My sister, Elizabeth, for her constant support and encouragement; my brother, for his unwavering help and belief in everything I do; and my parents, Hermann and Sheryl, for their unconditional love and support throughout my entire academic journey. I would not be here without them.

Other acknowledgments: I need to thank Fabiana Aellos, for her commitment as a friend, research mentor, and postdoctoral fellow on this project; none of this would have been possible without her, and I am profoundly thankful for all of her support. I would also like to thank: Julia Dworan, Giacomo Fabbri, Kasidy G. Harder, Stefano Boccardo, Pedro L. Cuevas, Isaiah Dawid, McKenna Vicini, Xue Yuan, Bo Liu, John B. Brunski, Romina Blanco, Meah Mccraw and Maria Casey for all of their contributions to this project. I would like to acknowledge the following funding sources: Osteology Foundation Young Researcher Grant (21-146), Max Kade Foundation 1221407-100-GHFXZ, and the Research Manitoba Master's Studentship Award 2023.

## Table of Contents

## INTRODUCTION

### *The barrier issue*

The primary function of epithelium in the body is protection, serving as a barrier between internal and external environments through a contiguous layer of cells. This epithelial barrier is the first line of defense against pathogenic insult, and when compromised, infection can ensue. In the oral cavity, teeth present a unique challenge to this protective system, as they transect the internal and external environments percutaneously: anchored in bone via ligaments at one end while exposed to the oral cavity for mastication at the other. The body addresses this unique challenge through the junctional epithelium (JE), a specialized epithelial barrier that adapts to adhere both to the tooth surface and to the adjacent oral epithelium and bone.

Like natural teeth, dental implants are also percutaneous and rely on a modified epithelial barrier, known as the peri-implant epithelium (PIE). Understanding the physiological differences between the JE and PIE, as well as the efficacy of the peri-implant soft tissue barrier, has become an increasing focus of research. Historically, implant success was primarily assessed by osseointegration, i.e., the direct structural and functional connection between bone and the implant. However, it is now well recognized that optimizing the soft tissue barrier is equally critical for the long-term success of dental implants. The literature strongly supports the importance of a stable soft tissue–implant interface in maintaining the longevity of bone-anchored prostheses (Abrahamsson et al., 1997; Berglundh et al., 1991, 2007; Ivanovski & Lee, 2018). However, our understanding of peri-implant soft tissue healing remains limited (Badillo-Perona et al., 2011; Kawahara et al., 1998).

The maturation of the PIE is influenced by multiple factors, including the biocompatibility of implant materials, the surgical technique, and the patient's ability to mount a robust repair response. A deeper understanding of how the peri-implant soft tissue interface forms and matures will ultimately inform strategies for improved soft tissue management around dental implants, enhancing their long-term stability and clinical outcomes.

### *Temporal characterization of the molecular events involved in mucointegration*

Clinical studies suggest that the dimensions of the peri-implant soft tissues remain stable during healing (Palombo et al., 2021). However, from a biological perspective, this region undergoes significant changes over time. Initially, an inflammatory response occurs, which, upon resolution, is followed by the deposition of an extracellular matrix that serves as a scaffold for fibroblast attachment and proliferation (reviewed in Sculean et al., 2014). These fibroblasts subsequently differentiate and produce a collagenous connective tissue that undergoes remodeling. The precise molecular mechanisms governing this remodeling phase remain unclear, particularly why this process is significantly slower than the initial healing phase.

Recent research has focused on the mechanisms by which soft tissues establish attachments to hard tissues, with the ultimate goal of applying these insights to improve the attachment of soft tissues to synthetic materials, including bone-anchored prostheses. For instance, it has been recently identified that a Wnt-responsive stem cell niche within the JE, which generates daughter

cells responsible for direct epithelial attachment to the enamel (Yuan et al., 2019). Wnt signaling from the JE is crucial for stabilizing hemidesmosomal proteins, which mediate soft-tissue attachment (Yuan et al., 2023). Furthermore, Wnt and other biological signals require mechanical input in the form of distortional strain to maintain both the stem cell niche and the attachment of JE to the tooth surface (Yuan et al., 2023).

Although histological similarities between the peri-implant epithelium (PIE) and JE are frequently emphasized (Sculean et al., 2014), important differences between these interfaces have been identified (reviewed in Ivanovski & Lee, 2018). For example, while the JE originates from the reduced enamel epithelium (REE) (Shimono et al., 2003), the PIE is derived from the oral epithelium (OE) (Yuan et al., 2021). Additionally, the cell proliferation rate within the PIE varies considerably depending on the healing stage (Yuan et al., 2021), whereas a consistently high mitotic index is a hallmark of an intact JE (Yuan et al., 2021, 2023; Yuan, Chen, Gauer, et al., 2020). These findings led us to conclude that PIE attachment to implant surfaces is suboptimal compared to the attachment of an intact JE to a tooth surface (Yuan et al., 2021).

***Implant surface influence on mucointegration***

Most strategies for improving implant integration have historically focused on surface modifications aimed at enhancing osseointegration (Aljateeli & Wang, 2013; Artzi et al., 2011; Javed et al., 2014). However, rather than osseointegration, the focus of this research is on mucointegration, the integration of peri-implant soft tissues.

A commonly held belief is that epithelial and connective tissues respond differentially to implant surface characteristics. However, in vitro studies have generally found negligible differences in cell attachment based on surface roughness (Abrahamsson et al., 2002; Berglundh et al., 2007; Bienz et al., 2021; Zitzmann et al., 2002). Meanwhile, in vivo data on the process of mucosal integration remain scarce. While peri-implant soft tissue dimensions and histological features have been described (Abrahamsson et al., 2002), and qualitative assessments of biopsied tissues surrounding different restorative materials have been conducted (Baus-Dominguez et al., 2024), to our knowledge, there are no quantitative in vivo studies that directly assess how the peri-implant epithelium (PIE) and connective tissues respond to different implant surfaces.

Implant surfaces have been modified using biomaterial coatings such as silver, copper, zinc, hydroxyapatite, and calcium phosphate. However, justifications for these modifications are often indirect. For instance, zinc deficiency is associated with impaired bone growth in rats, leading some investigators to hypothesize that zinc might enhance osseointegration (Qiao et al., 2014), though this remains debated (see Zhao et al., 2021). Hydroxyapatite (HA), the primary mineral component of enamel to which the JE adheres, is known for its biocompatibility. However, when applied as a coating on titanium implants, HA has been shown to delaminate (Arcos & Vallet-Regi, 2020; Ferraris & Spriano, 2016). Whether mucosa attaches more effectively to HA than to titanium remains unknown.

Another surface modification strategy involves using noble alloys, which appear to reduce biofilm formation (Meier et al., 2023). While this suggests a potential clinical benefit, no preclinical or clinical data currently exist to support or refute this claim.

Anodization is an electrochemical process that creates a porous oxide layer on titanium surfaces. Many studies have suggested that anodization improves both hard and soft tissue integration, but these conclusions are predominantly based on in vitro studies (Albrektsson, 2019; Wennerberg et al., 2018). However, extrapolating in vitro findings to clinical performance is inherently challenging (Sugawara et al., 2016). Recognizing this limitation, we sought to develop an in vivo model capable of deeply interrogating the soft tissue–implant interface using molecular markers.

This background motivated our investigation of two clinically relevant questions:

1. **Does soft tissue barrier formation differ between immediate and delayed implants?** We focus on characterizing the molecular events underlying these different placement protocols.
2. **Do implant surface properties influence peri-implant soft tissue barrier formation?** We evaluate the role of abutment surface material in endosseous implant integration.

These questions are explored in Parts I and II of this manuscript, respectively.

## Part I: Dynamic analyses of a soft tissue–implant interface: Biological responses to immediate versus delayed dental implants

### *Introduction*

A 2014 consensus report from the 10th European Workshop on Periodontology suggested that the PIE may differ depending on whether an implant is placed in a fresh extraction socket (immediate placement) or in a healed site (delayed placement) (Hämmerle, Giannobile, & Working Group 1 of the European Workshop on Periodontology, 2014). This statement motivated our investigation into whether the formation of the soft tissue–implant interface varies between these two placement protocols. In this study, we examined not only the formation of the PIE but also how peri-implant connective tissues respond during the process of mucointegration. Additionally, we significantly extended the timeframe over which PIE maturation was analyzed, allowing us to capture a more comprehensive picture of the molecular mechanisms governing soft tissue attachment. These analyses provided critical new insights into the biological processes underlying the maturation of the soft tissue–implant interface.

### *Materials and Methods*

#### *Mice*

All experimental protocols were approved by the Stanford Committee on Animal Research under protocol #13146, and by Bannatyne Campus Animal Care Committee (BC ACC) at University of Manitoba, and were conducted in accordance with ARRIVE guidelines. The study included three experimental groups and one control group:

- Immediate implant group (*N* = 19): ~6-week-old mice underwent extraction of the first maxillary molars (mxM1), followed by immediate implant placement.
- Delayed implant group (*N* = 4): ~6-week-old mice underwent mxM1 extraction, allowed for site healing, and later received an implant.
- Extraction group (*N* = 8): ~6-week-old mice underwent mxM1 extraction without subsequent implantation.
- Control group (*N* = 3): ~6-week-old mice underwent no procedures, serving as a benchmark for an intact JE (see Table 1).

All mice were housed in a temperature-controlled environment with a 12-hour light/dark cycle and provided with food (hard diet) and water ad libitum.

For all experimental groups, mice were anesthetized intraperitoneally with ketamine (100 mg/kg body weight) and xylazine (10 mg/kg body weight). Analgesia was maintained using subcutaneous Buprenorphine SR (slow release; 1.5 mg/kg body weight). Bilateral mxM1 extractions were performed using micro-forceps, and hemostasis was achieved by local compression. All surgeries followed sterile surgical techniques.

#### *Immediate implant placement*

Immediately following extraction, 0.62-mm-diameter screw-shaped titanium alloy implants (Ti-6Al-4V) with a machined surface (Retopins, NTI Kahla GmbH) (Blanc-Sylvestre et al., 2021) were manually placed into the palatal root sockets of the extracted mxM1s. Implants were positioned

~0.6 mm above the alveolar ridge and gingiva in a sub-occlusal position. Cutting pliers were used to separate the implants from their handle.

### *Delayed implant placement*

For the delayed implant group, mxM1 extractions were performed two weeks prior to implant placement. At the time of implantation, flapless osteotomies were prepared in the healed mxM1 sites using: (1) A 0.38-mm drill (Drill Bit City, USA) at 1000 rpm to create a pilot hole. (2) A handheld 0.48 mm drill to enlarge the osteotomy. The implants were then manually placed in a sub-occlusal position, ~0.6mm above the alveorlar ridge.

Soft tissue healing was evaluated at post-implant days (PID) 1, 3, 7, 14, and 28. No evidence of infection or prolonged inflammation was observed at the surgical sites or around the implants. No antibiotics were administered to the operated animals. Additional details on materials and methods are provided in the Appendix Part I Data.

### *Results*

#### *Soft tissue maturation around immediate and delayed implants appears equivalent.*

A rodent model was employed to evaluate mucosal integration of titanium alloy implants. Immediately after an implant is placed into a fresh extraction socket, the interface largely consists of an injured JE and a blood clot (Fig. 1A). Within 3 days, the peri-implant wound appeared to have healed; between 7 and 14 days, it is difficult to appreciate color differences between the healing soft tissue-implant interface and adjacent OE (Fig. 1A). In a rodent model of delayed implant placement, soft and hard tissue healing around the implant appeared clinically indistinguishable from healing around an immediate implant (Fig. 1B). These features of soft tissue healing around implants in rodents were similar to soft tissue healing around implants in patients (Appendix Part I, Fig. 1A).

#### *Histological maturation of the soft tissue interface around immediate and delayed implants appears equivalent.*

Histology helped clarify soft and hard tissue healing responses that had been observed clinically. Around a delayed implant, the initial soft tissue-interface is formed during extraction socket healing; therefore, our analyses focused first on this repair program. On post-extraction day (PED) 1, a blood clot filled the extraction site (Fig. 1C); on PED3 the clot became organized and re-epithelization began (Fig. 1D). By PED7, the edge of the healing epithelium covering the socket was distinguished from the intact OE (arrow, Fig. 1E). By PED14 only OE remained (Fig. 1F). At this timepoint, bone filled the extraction site and remodeling was underway; it was into this site that a delayed implant was placed.

Next, we compared soft tissue healing around these delayed implants with healing around immediate implants. Around immediate implants, remnants of the Periostin-positive periodontal ligament (PDL) remained after tooth extraction (asterisks, Fig. 1G and Appendix, Part I Fig. 1B), which would eventually contribute to the hard tissue-implant interface. Remnants of the JE contributed to the soft tissue-implant interface, as shown by expression of the JE marker, epCAM (Appendix Part I, Fig. 1C). Around delayed implants the PDL and JE no longer exist and thus made no contribution to the muco- and osseo-integration process.

Other aspects of soft tissue healing were indistinguishable i.e., re-epithelialization took place at the same rate whether an implant was present or not (compare Fig. 1D,E,F with H,I,J). By PID14, the soft tissue-interface around an immediate implant (Fig. 1J) was histologically indistinguishable from that around a delayed implant (Fig. 1N). Both delayed and immediate implants were osseointegrated by PID14 (Appendix, Part I, Fig. 1D,E).

*Temporal formation and organization of healing peri-implant connective tissues.*

Peri-implant connective tissues were assessed next. Vimentin expression, which identifies class-III intermediate filaments in the connective tissue, was evaluated. Compared to the lamellar organization of Vimentin+ fibers in supracrestal tissues around teeth (Fig. 2A), Vimentin+ cells in the peri-implant soft tissues were randomly distributed (Fig. 2B). Between PID3 and PID7, the number of Vimentin+ cells appeared to increase but the cells were not aligned in a linear pattern (Fig. 2C). Vimentin expression appeared to increase still further by PID14 but still no aligned pattern of the immunopositive cells emerged (Fig 2D).

Collagen orientation and density in the peri-implant connective tissues was assessed using picrosirius red staining. Compared to the dense, mature (red-fluorescing) collagen fibers in the connective tissue around teeth (Fig. 2E), significantly less collagen formed in the connective tissue around implants (Fig. 2F,G,H; quantified in I). Peri-implant collagen was also significantly less organized, even at later timepoints e.g., PID14 (Fig. 2I). In comparison, implants were fully osseointegrated by PID14 (Appendix Part I, Fig. 1).

The distribution of Vimentin+ cells around delayed implants was similar to that seen around immediate implants, with immunopositive cells being scattered throughout the connective tissues (Fig. 2J,K). On PID14 Vimentin+ cells appeared to increase (Fig. 2L). Quantitative analyses confirmed a significantly less mature, less dense collagen content in the connective tissue around delayed implants (Fig. 2M-O; quantified in I).

*Hemidesmosomal attachment protein expression gradually increases with time in the PIE-connective tissue interface, and in the PIE.*

Quantitative IHC was used to compare hemidesmosomal protein expression in the PIE. During early wound repair, hemidesmosomal laminins and integrins are involved in re-epithelialization and specifically in the interactions between wound keratinocytes and the underlying connective tissue matrix; accordingly, the first site of Laminin5 expression in the soft tissue-implant interface was in the basement membrane between the connective tissue and OE (asterisk, Fig. 3A). At this timepoint, the PIE itself was devoid of Laminin5 expression (Fig. 3A; quantified in D). By PID7, Laminin5 persisted in the basement membrane but was largely absent from the PIE (Fig. 3B). By PID14, Laminin5 was detected in the PIE (arrow, Fig. 3C; inset) and was no longer expressed in the basement membrane (Fig. 3C).

The expression levels of Laminin5 was then quantified as a function of time and its location. Although initially very strongly expressed in the basement membrane, Laminin5 in the actual PIE was virtually non-existent at PID3 and PID7 (Fig. 3D). By PID14, Laminin5 expression levels had increased significantly in the PIE (Fig. 3D). Laminin5 expression around a delayed implant was qualitatively equivalent to that around immediate implants (Fig. 3E).

Expression of a second hemidesmosomal protein, ß4 integrin was assessed as an indicator of soft tissue attachment to the implant. The distribution of ß4 integrin+ cells followed a pattern similar to Laminin5 (asterisk, Fig. 3F; quantified in I). For example, on both PID3 and PID7, ß4 integrin was expressed in the basement membrane but was deficient in the PIE (Fig. 3G). By PID14, weak ß4 integrin expression was detectable in the PIE (Fig. 3H). Quantification and ß4 integrin+ cells followed a trend of gradually increasing in the PIE, but the increases were not statistically significant (Fig. 3I). ß4 integrin expression around a delayed implant was qualitatively equivalent to that around an immediate implant (Fig. 3J). A third hemidesmosomal protein, Plectin, also initially showed diffuse expression in the healing basement membrane and connective tissues around the implants, and initially weak expression in the PIE (Fig. 3K). Unlike the other hemidesmosomal proteins, quantification of Plectin expression levels increased significantly between PID7 and PID14 (Fig. 3L,M,N). Plectin expression around immediate and delayed implants was similar (Fig. 3O).

### *The PIEs around immediate and delayed implants continue to mature long after osseointegration is complete.*

On PID14, delayed and immediate implants were fully osseointegrated (Appendix Part I, Fig. 1) but molecular analyses of attachment proteins indicated weak expression in the PIE. To determine if their expression levels increased at later timepoints, we continued analyses until PID28. At this timepoint, some- but not all- samples exhibited a pronounced improvement in the histologic appearance of the PIE (compare Fig. 4A with B,C). Quantitative analyses also indicated that by this timepoint, supracrestal tissue thickness had stabilized around implants (Fig. 4D). Quantitative PCNA IHC demonstrated that by PID28, cell proliferation in the PIE was on par with that observed in an intact JE (compare Fig. 4E with F,G; quantified in H).

The distribution and level of attachment proteins were both re-assessed on PID28. Laminin5, ß4 integrin and Plectin-positive cells were generally positioned facing the tooth/implant surfaces (Fig. 4I-S). Compared to expression levels in an intact JE, expression in the PIE remained significantly lower (Fig. 4L,P,T).

One indicator of an effective barrier is the degree to which oral pathogens are prevented from accessing the peri-implant connective tissues. We used the distribution and number of CD68-positive macrophages in the connective tissues underlying the PIE as an indication of an effective barrier. As anticipated, when the soft tissue-implant interface was immature e.g., PID3, CD68 expression was high in the connective tissue (Fig. 4U). As the soft tissue-implant interface completed re-epithelialization e.g., on PID7, CD68 expression was reduced (Fig. 4V). By PID14, CD68 expression in peri-implant connective tissues was significantly lower (Fig. 4W). By PID28, the distribution of CD68+ macrophages in the peri-implant environment were on par with that seen around an intact JE (Fig. 4X; quantified in Y).

## *Discussion*

Bone-anchored percutaneous implants are amongst the most common medical devices in use today. Despite decades of innovation to improve prosthetic functionality (Kulkarni et al., 2023; Montero, 2021), infection at the soft tissue-implant interface has been, and continues to be, the chief cause of implant failure (reviewed in (Atallah, Leijendekkers, Hoogeboom, & Frolke, 2018;

Li & Fellander-Tsai, 2021; Overmann et al., 2020)). Indeed, creating "a material for [the] interface that would provide an absolute bacterial barrier, being tenacious in its attachment, and having the strength and durability for long-term function" (Hall, 1974) still remains a critical- and largely unmet- medical need. In this study we focused on understanding how the soft tissue-implant interface forms and matures over time, with the ultimate goal to improve its barrier functions and protect against peri-implant disease.

### *The PIE around immediate versus delayed implants: similar or different?*

A consensus report published a decade ago tentatively suggested that "peri-implant junctional epithelium may reach a greater final length [around] implants placed into fresh extraction sockets versus conventional implant procedures in healed sites" (Hammerle et al., 2014). This speculation prompted us to evaluate the extent to which the PIE around a delayed implant differed from the PIE around an immediate implant (Fig. 2). Qualitatively, the rate of mucosal integration between immediate and delayed implants was equivalent, despite the fact that the former consisted of an entire extraction socket and the latter was a size-adjusted osteotomy (Fig. 1). The only notable difference was the contribution of PDL cells to osseointegration, and JE cells to mucointegration, of an immediate implant, which was lacking in the delayed implants (Appendix Part I, Fig. 1, and (Yuan et al., 2018)). It is tempting to speculate that given the robustness with which the JE responds to injury (Yuan, Chen, Van Brunt, et al., 2020), an immediate implant might develop a more mature PIE faster than a delayed implant but at present, this remains a conjecture.

### *Potential role(s) for the connective tissues in PIE maturation*

Around teeth, the connective tissue has an influence on the characteristics of the overlying epithelium (Imber et al., 2023),(Lu, Hobbs, Dyer, Ghuman, & Hughes, 2020). Around implants, connective tissues may also have an influence on the PIE (Ramanauskaite, Schwarz, & Sader, 2022). From our quantitative analyses, connective tissue maturation is a much slower process than re-epithelization (Fig. 2) (Singh, Rai, & Agrawal, 2023). For example, even at a timepoint when osseointegration is accomplished e.g., PID14, the amount of mature collagen in the peri-implant environment is a fraction of that found in connective tissue around teeth (Fig. 2I). Regardless of whether the implant is immediate or delayed, qualitative assessment of Vimentin expression showed a pattern of disorganized cells in the peri-implant environment, unlike the linear array seen in intact connective tissue around teeth (Fig. 2). During peri-implant wound healing, Vimentin+ intermediate filaments provide the scaffold to support fibroblast migration into the environment, but even on PID14, a linear pattern was not obvious (Fig. 2D,L). Vimentin+ cells also help maintain the structural integrity and resilience of peri-implant tissues to mechanical forces but in the peri-implant environment, the lack of an organized Vimentin+ intermediate filament matrix suggested that the tissues were still fragile in comparison to intact controls (Fig. 2B-D, J-L). It should be noted, however, that these implants were not functionally loaded, which is known to influence connective tissue density and organization around teeth. However, it remains somewhat controversial if this has an impact on collage fiber orientation in the periimplant enrionment (Rocci et al., 2003)

### *Distinct stages of PIE formation and maturation are revealed by analyses of hemidesmosomal proteins.*

Initially, hemidesmosomal proteins are expressed in the healing basement membrane around implants (Fig. 3), a finding that comports with the literature on hemidesmosomal function during wound healing (Iorio, Troughton, & Hamill, 2015; Martins-Green, 2013). At the wound, epithelial cells must both adhere to the underlying connective tissue while simultaneously migrating across it to repair the injury. In this regard, hemidesmosomal proteins including laminins and integrins seem essential for establishing a soft tissue barrier around implants. In keeping with this hypothesis, the hemidesmosomal proteins Laminin5, ß4 integrin, and Plectin were strongly expressed in the peri-implant basement membrane on PID3 and PID7 (Fig. 3).

Over time, their expression domains gradually shifted from the basement membrane to the PIE proper, where presumably their functions were to mediate an attachment to the implant surface, much like they do to a tooth surface. At PIEs examined from PID3 to PID28, quantitative analyses of hemidesmosomal protein levels remained significantly reduced compared to an intact JE (Fig. 3,4). From these data we conclude that a PIE has a significantly weaker hemidesmosomal-mediated attachment compared to an intact JE. This does not eliminate the possibility that the soft tissue attachment to an implant is mediated by different (currently unknown) proteins.

### *A model to explain the rate of PIE maturation.*

Soft tissue repair after gingivectomy is estimated to take ~2 weeks (Novaes, Kon, Ruben, & Goldman, 1969; Waerhaug, 1978) while maturation of the PIE-as assessed by histology- is thought to take 6-8 weeks (Berglundh et al., 2007; Tomasi et al., 2014). Why is PIE maturation so much slower that epithelial maturation around teeth? Some investigators have stated that soft tissue healing around an implant is akin to a ‘foreign body reaction’ but this statement fails to provide insights into what factors- biological and physical- are controlling the rate of PIE maturation versus epithelial healing around teeth.

Although the clinical literature provides scant clues as to why PIE maturation is so much slower that healing around teeth, our molecular analyses suggest a plausible explanation. Using a variety of injury repair models, we demonstrated that oral epithelial repair is generally made possible by tissue-resident stem cell niches (Yuan, Chen, Gauer, et al., 2020; Yuan, Chen, Van Brunt, et al., 2020; Yuan et al., 2019),(Byrd et al., 2019). Under homeostatic conditions, these epithelial niches produce daughter cells that contribute to the continual turnover of the epithelia (Yuan, Chen, Gauer, et al., 2020; Yuan, Chen, Van Brunt, et al., 2020; Yuan et al., 2023; Yuan et al., 2019),(Byrd et al., 2019),(Tanaka et al., 2021). In response to injury e.g., extraction of a tooth, gingivectomy, and placement of an implant, these same epithelial niches dramatically increase production of mitotically active daughter cells, which then migrate widely to occupy and heal the damaged areas (Yuan, Chen, Gauer, et al., 2020; Yuan, Chen, Van Brunt, et al., 2020; Yuan et al., 2021b). Unlike an injured JE, however, the PIE lacks an equivalent epithelial stem cell niche (Yuan et al., 2021b). Instead, the initial generation of mitotically active daughter cells comes from the adjacent OE, where cells must migrate over distances to occupy the peri-implant environment (Yuan, Chen, Van Brunt, et al., 2020). This migratory requirement constitutes a plausible explanation for the protracted maturation of soft tissues around an implant versus maturation of soft tissues around teeth.

What remains unclear is why the PIE at PID28 still differs substantially from an intact JE. Is a different cell population involved in late-stage PIE remodeling? And if so, from where does this

second cell population originate? We know something about the mechanisms, both physical and/or biological, that contribute to establishment of a JE stem cell niche (Yuan et al., 2023); could these same factors be re-activated to create a stem cell niche around implants? These questions form the basis of ongoing investigations by our group into methods to accelerate and rejuvenate barrier functions to the PIE.

### *Limitations and Conclusions*

There are three notable limitations to this study. The first is that the study was carried in rodents and the extent to which rodent data reflect the human condition depends upon having access to equivalent peri-implant tissues from patients. For ethical reasons, the collection of peri-implant soft tissues during early stages of mucosal integration is contraindicated. Consequently, our understanding of PIE maturation and its barrier functions are currently restricted to results from animal studies.

A second limitation is that there was a significant amount of variability in the expression levels of attachment proteins in the developing PIE (Figs. 3,4). The reason(s) for this variability are at present unknown. Even though the number of samples was large, oftentimes statistical significance was only reached when comparing samples from PID3 and PID28. As a consequence of this variability, we were cautious about drawing strong conclusions about attachment mechanisms from these data. Ongoing studies are focused on identifying the cause(s) of this variability, which may be related to the fact that the implant had to be removed for tissue processing. We are currently investigating methods to circumvent this difficulty.

Within the limitations of the current study, we conclude the following: first, histological, and quantitative molecular assessments together suggest that PIE maturation is equivalent around immediate and delayed implants. Second, quantitative analyses demonstrated that connective tissue maturation never reached that observed around teeth. However, the implants placed in this study were never functionally loaded, which may have influenced this finding. Third, hemidesmosomal proteins that mediate the JE attachment to the tooth surface are expressed at lower levels in the PIE, suggesting a weaker barrier. There is a caveat, however: the density of macrophages was gradually decreased in the peri-implant environment, suggesting that the barrier functions of the PIE continued to improve as a function of time. Therefore, we posit that hemidesmosomal proteins may not be the sole molecules by which the PIE attaches to an implant surface. We continue to explore the expression of other types of adhesion molecules for their roles in mediating the soft tissue attachment to an implant surface.

## *Figures and Figure Legends*

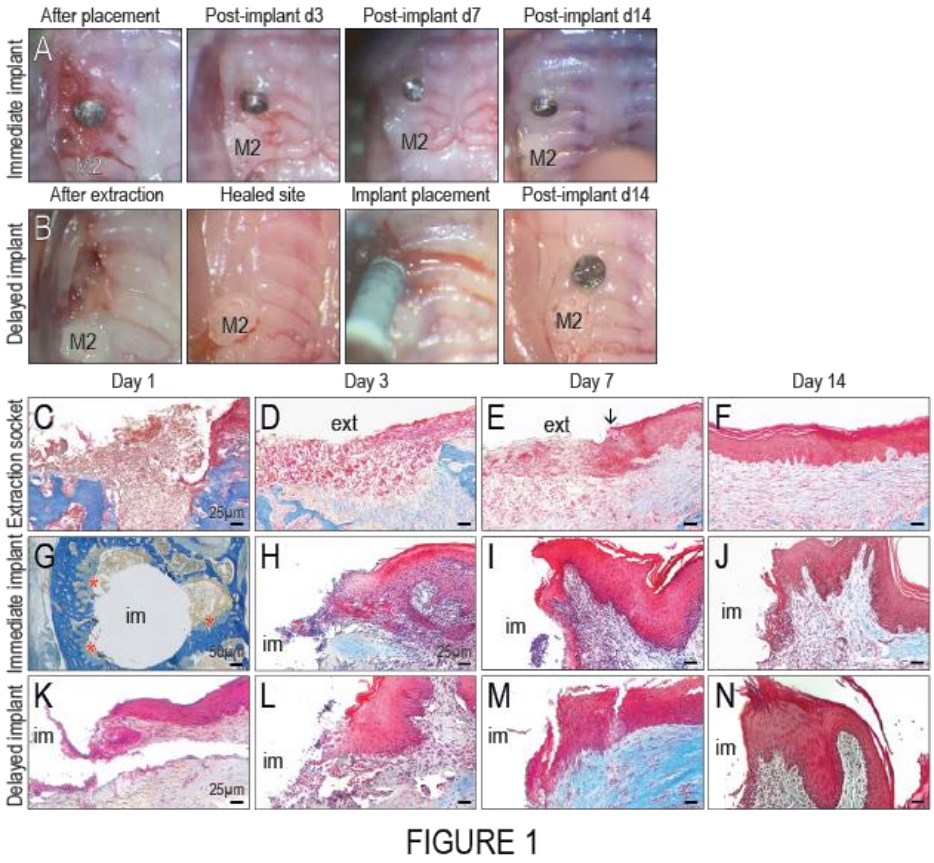


FIGURE 1

**Figure 1. Mucosal integration process over time in patients compared with a preclinical animal model**

(A) Sequence of intraoral clinical photographs of immediate implants after placement, and on post-implant day 3, 7, and 14. (B) Sequence of intraoral clinical photographs of delayed implant placement, beginning after tooth extraction, followed by socket healing, then by implant placement and post-implant day 14. (C) Masson's trichrome-stained sagittal tissue sections through an extraction socket, 24h after tooth removal. (D) On post-extraction day 3 (PED3), epithelial cells cover the socket; (E) on PED7, a loose epithelia covers a clot-filled socket; (F) by PED14, the initial stage of epithelia and connective tissue healing appears complete. (G) Masson's trichrome-stained transverse tissue section of the immediate implant bed, where remnants of the PDL can be visualized in the sockets. (H) By PID3, epithelia are in contact with the immediate implant surface and (I) by PID7, an initial PIE has formed. (J) At PID14, the PIE around an immediate implant. (K) Masson's trichrome-stained transverse tissue section of the delayed implant bed, with minimal epithelium present at the implant surface. (L) By PID3, the epithelia is in contact with the delayed implant surface and has several cell layers. (M) By PID7, a distinct PIE has formed with the delayed implant surface which is histologically matured compared to (I). (N) At PID 14, the delayed and immediate implant PIE are histologically similar. Scale bars: as indicated. Abbreviations: im, implant; pie, peri-implant epithelium; oe, oral epithelium; ext, extraction site; M2; second maxillary molar.

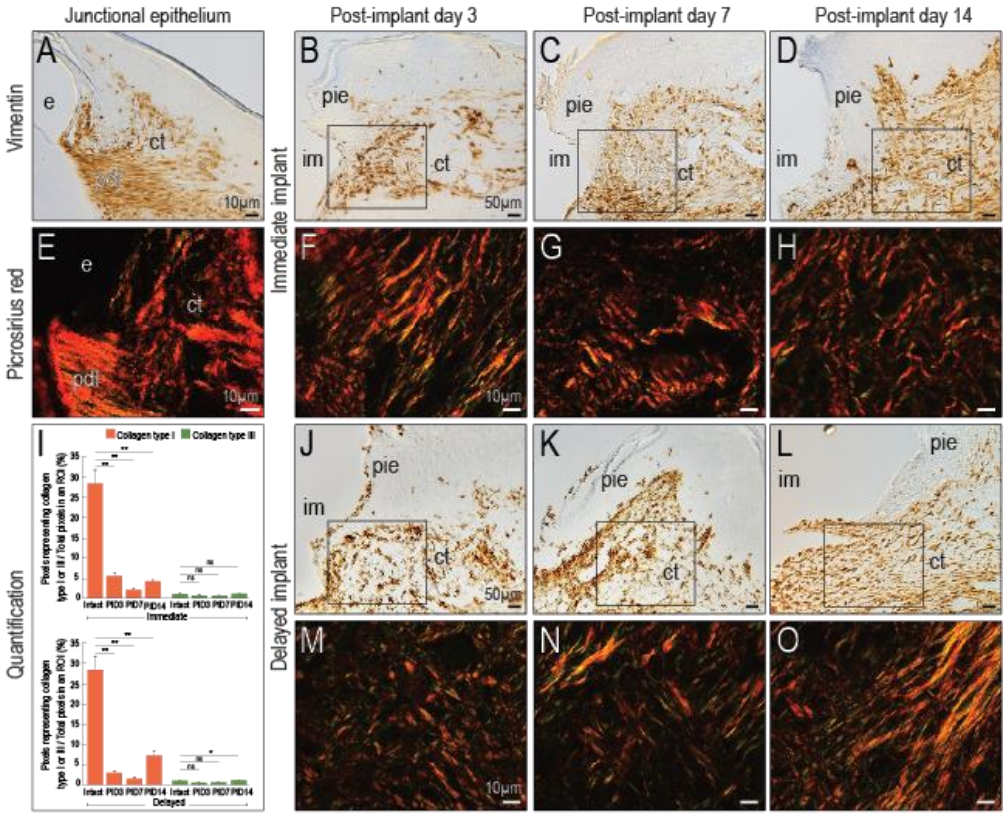


FIGURE 2

**Figure 2. Comparison of collagen fiber distribution and maturation in a healing PIE versus a JE**

(A) Expression of Vimentin-positive intermediate filaments in the connective tissue around teeth, and around immediate implants on (B) PID3, (C) PID7, and (D) PID14. When viewed under polarized light, picrosirius red-stained tissue sections of the (E) tooth show mature supracrestal collagen fibers whose birefringence appears orange-red. The birefringence of less mature (e.g., green) collagen fibers in the connective tissues around immediate implants on (F) PID3, (G) PID7, and (H) PID14. (I) Quantification of orange-red (type I) and green (type III) fluorescing collagen in the connective tissue around teeth, and in the connective tissue around immediate implants and delayed implants. (J) Vimentin-positive intermediate filaments in the connective tissue around delayed implants on PID3, (K) PID7, and (L) PID14. Picrosirius red-stained tissue sections of collagen fibers in the connective tissues around immediate implants on (M) PID3, (N) PID7, and (O) PID14. Scale bars: as indicated. Abbreviations: epi; epithelium, ct, connective tissue; im, implant; pie, peri-implant epithelium.

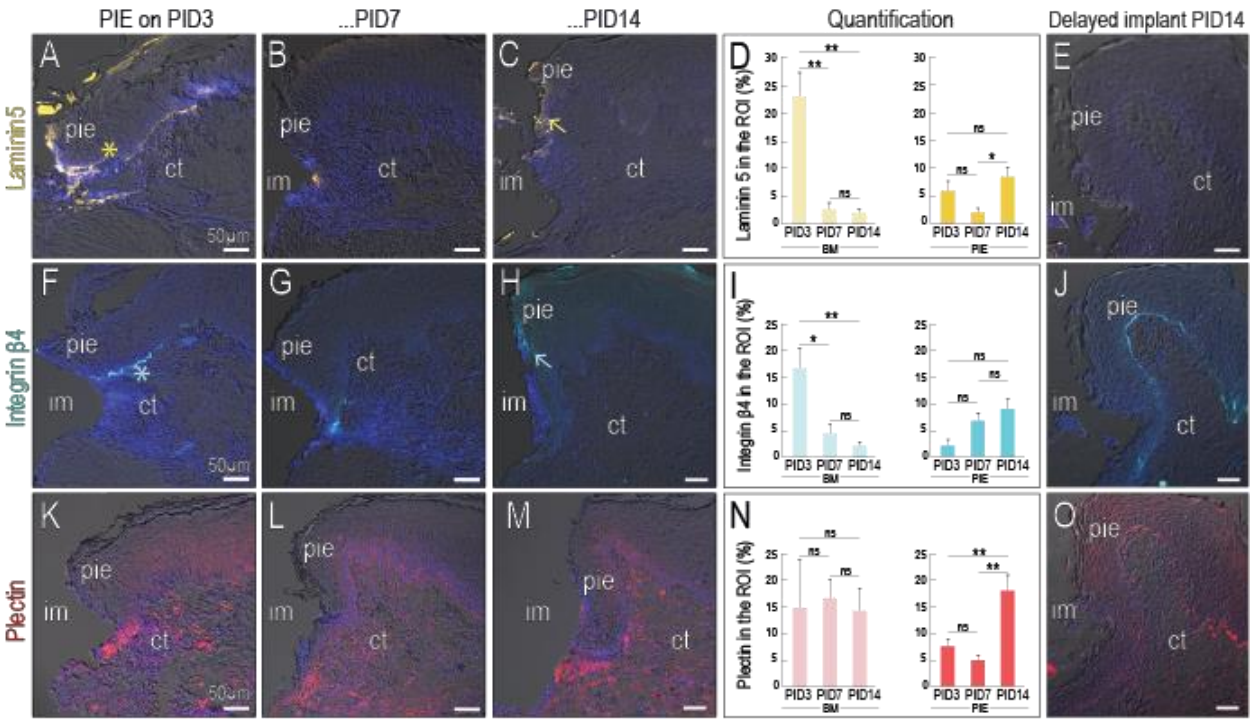


FIGURE 3

**Figure 3. Hemidesmosomal proteins are weakly expressed in the maturing PIE.**

Around a representative immediate implant, expression of the hemidesmosomal attachment protein Laminin5 on (A) PID3 (B) PID7, and (C) PID14. (D) Quantification of Laminin5 expression in the basement membrane (BM) and in the peri-implant epithelium (PIE) at timepoints indicated in. (E) Expression of Laminin5 in the PIE around a delayed implant on PID14. Around a representative immediate implant, expression of the hemidesmosomal attachment protein ß4 integrin on (F) PID3 (G) PID7, and (H) PID14. (I) Quantification of ß4 integrin expression in the BM and PIE at timepoints indicated in. (J) Expression of ß4 integrin in the PIE around a delayed implant on PID14. Around a representative immediate implant, expression of the hemidesmosomal attachment protein Plectin on (K) PID3 (L) PID7, and (M) PID14. (N) Quantification of Plectin in the BM and PIE. (O) Expression of Plectin in the PIE around a delayed implant on PID14. Scale bars: as indicated. Abbreviations: im, implant; pie, peri-implant epithelium; ct, connective tissue.

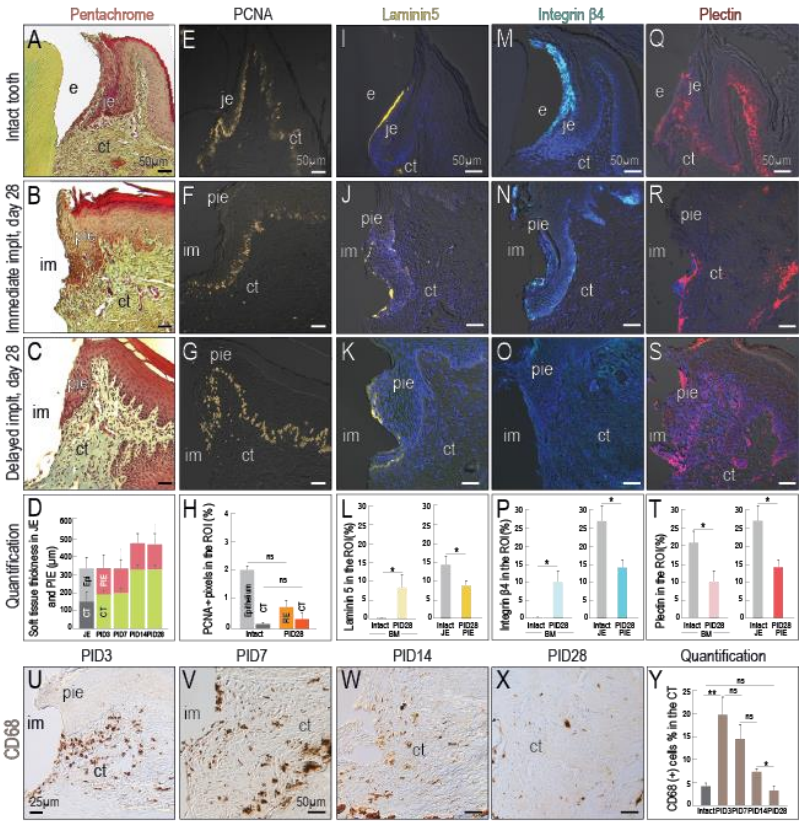


FIGURE 4

**Figure 4. A mature PIE expresses higher levels of attachment proteins, a stable connective tissue width, and an immune response similar to an intact JE.**

Representative Movat's pentachrome-stained section of (A) an intact JE compared to the PIE at PID28 around an (B) immediate and (C) delayed implant. (D) Quantification of immediate implant. PCNA expression illustrates the distribution of mitotically active cells in (E) an intact JE compared to the PIE at PID28 around an (F) immediate and (G) delayed implant. (H) Quantification of PCNA+ cells in JE and connective tissue around a tooth and in the soft tissue-implant interface of an immediate implant (PIE and connective tissue). Laminin5 expression illustrates the (I) attachment of the JE to the tooth surface compared to the attachment of the PIE at PID28 to (J) an immediate and (K) delayed implant. (L) Quantification of Laminin5+ cells in the JE, and BM and PIE around an immediate implant on PID28. ß4 integrin expression illustrates the (M) attachment of the JE to the tooth surface compared to the attachment of the PIE at PID28 to (N) an immediate and (O) delayed implant. (P) Quantification of ß4 integrin+ cells in the JE, and BM and PIE around an immediate implant on PID28. Plectin expression illustrates the (Q) attachment of the JE to the tooth surface compared to the attachment of the PIE at PID28 to (R) an immediate and (S) delayed implant. (T) Quantification of Plectin+ cells in the JE, and BM and PIE around an immediate implant on PID28. Expression of CD68 in the connective tissue (U) PID3, (V) PID7, (W) PID14, and (X) PID28. (Y) Quantification of CD68+ cells in the connective tissue around a tooth, and in the connective tissue around immediate implants at the timepoints indicated. Abbreviations: im, implant; pie, peri-implant epithelium; ct, connective tissue.

## Part II: Dynamics of mucosal integration of machined vs. anodized titanium implants

### *Introduction*

Implant anchorage depends on interfacial bonding between bone and the implant. What is often overlooked- but no less important for long-term implant success- is the interfacial attachment between the implant and soft tissues (Sculean et al. 2014). The nature of this soft tissue-implant interface is only now being deciphered at a molecular level (Aellos et al. 2024). This work aims to develop a quantitative understanding of the biological factors that influence soft tissue integration of dental implants.

Large animal models including mini pigs and dogs allow a full-size implant with fully characterized surfaces can be evaluated but because such studies only include a limited number of timepoints for analysis, they can offer only a "snapshot in time" of mucosal integration. To better understand the entire process of mucosal integration, from the time of implant placement to maturation of the interface, we turned to a rodent model that is amenable to genetic, molecular, and cellular manipulation and analyses. Aside from technical challenges, this model has been successfully used to evaluate osteotomy site preparation tools (Coyac et al. 2019), the biology (Coyac et al. 2020) and biomechanics of implant osseointegration (Tian et al. 2022), and most recently, the formation (Yuan et al. 2021) and maturation (Aellos et al. 2024) of the soft tissue-implant interface.

### *Materials and Methods*

#### *Experimental design*

A flowchart is shown in Appendix Part II, Fig. 4, demonstrating the split-mouth design of the study. An intact, healthy JE around the maxillary first molar (mxM1) was used for comparisons between a soft tissue-implant vs. a soft tissue-tooth interface.

#### *Mice and surgeries*

All procedures conformed to ARRIVE guidelines. Implants were placed in fresh extraction sockets, then analyzed at multiple timepoints to capture the dynamic process of mucosal integration. Please see Appendix Part II data for details of tooth extraction, miniatured implants, implant placement, and the distribution of mice including their strains/genders in Table 1.

#### *Patient information, tissue processing, analyses of surface characteristics, staining protocols, statistics, and methods of quantification*

Please see Appendix Part II data.

### *Results*

#### *The abutment surface of a mouse-sized implant is modified by anodization*

Miniaturized titanium alloy implants were either maintained with a machined surface , which has been shown to accumulate less bacteria than a rough surface (Schmidlin et al. 2013), or were coated with a titanium oxide layer via a mild anodization process, to align with some implants in clinical practice today. The anodized surface extended from the apex of the implant to its top e.g., the platform. Anodization can sometimes change the texture of an implant surface;

therefore, SEM was performed to assess whether the electrochemical reaction created a nano-texture. SEM analyses verified that machined surfaces were smoother than anodized surfaces (Fig. 1A,A', B,B'). Anodized surfaces were covered with nanometer-sized pores that were absent from machined surfaces (Fig. 1C,D). Surface chemistry characterization revealed an oxygen:titanium ratio that was ~six-fold higher in anodized implants; all other ratios e.g., aluminum:titanium and vanadium:titanium were similar (Fig. 1E,F; quantified in G). Thus, anodization did not change the bulk material but only the abutment surface to which peri-implant cells were exposed.

### *The temporal course of mucosal integration is established.*

Most implants have an abutment component that is separate from the body of the implant (Fig. 2A). Typically, the abutment component has a surface that is distinct from the surface characteristics of the body component. Due to their size, however, murine implants were manufactured such that to the body and abutment components were combined into a single integrated implant, and the surface characteristic e.g., machined or anodized, stretched from the platform to the apex of the implant (Fig. 2A).

Corresponding to an immediate implant protocol in patients, murine implants were placed in fresh extraction sockets (Fig. 2A). The first analyses were focused on assessing osseointegration. On post-implant day 3 (PID3), the peri-implant environment around all implants was largely comprised of a fibrin-rich blood clot (upper left panel, Fig. 2B). By PID7, a densely cellular tissue surrounded the implant body (upper right panel, Fig. 2B). By PID14, the body portion of all implants were surrounded by bone (lower left panel, Fig. 2B). By PID28, the appearance of the peri-implant bone was unchanged (lower right panel, Fig. 2B).

The amount of peri-implant bone was quantified. Compared to PID3 and PID7, where the bone-implant contact (BIC) was <40%, on PID14, the BIC was 72% (Fig. 2C). There was no significant difference in the BIC between PID14 and PID28 (Fig. 2C). From these data we concluded that osseointegration was achieved by PID14, and that implants remained osseointegrated for the duration of the experiments.

### *Barrier functions of the PIE are comparable between machined and anodized implant/abutment surfaces*

PIE barrier functions were evaluated next, using two metrics. First, attachment of soft tissue to the implant surface was evaluated using qIHC for the hemidesmosomal protein, Laminin5. Laminin5 is part of the JE attachment apparatus (Fig. 3A). On PID3, Laminin5 expression was not detected in the PIE around both implants; rather, its expression was restricted to the basement membrane (Fig. 3B,C). This pattern aligns the role of Laminin5 in wound healing, where it mediates adhesion between migrating epithelial cells and underlying connective tissue. Laminin5 continued to be weakly expressed on PID7 in the basement membrane around both implants (Fig. 3D,E).

By PID14, the first signs of Laminin5 expression appeared in the PIE (Fig 3F,G). Expression levels of Laminin5 were significantly lower in the PIEs than in a JE (Fig. 3H). One observation of note was that on PID14, Laminin5 expression was significantly higher around anodized implant surfaces (Fig. 3H).

The macrophage marker CD68 was also used to assess PIE barrier functions. In the JE, CD68 was detected in cells scattered throughout the connective tissue (Fig. 3I). Around implants on PID3, CD68-positive cells were abundant throughout the connective tissues, with no significant differences noted between implant surfaces (Fig. 3J,K; quantified in P). Expression levels of CD68 were unchanged on PID7, again with no significant differences between the surfaces noted (Fig. 3L,M; quantified in P). By PID14, the number of CD68-positive macrophages was significantly decreased (Fig. 3N,O), equivalent to that found around a healthy JE (Fig. 3P). The number of CD68-positive cells was not significantly different around machined implants vs. anodized implants (Fig. 3P).

### *Peri-implant soft tissues respond similarly to machined and anodized abutment surfaces, but both improve significantly with time.*

In clinical practice, removal of an anodized abutment at post-implant week 10 often produces some bleeding (Fig. 4A) and sometimes, remnants of the PIE remained adherent to the implant (Fig. 4B). A subset of machined and anodized implants was removed from mice at PID28 and they showed a similar feature, with soft tissue remnants adhering to the implant (Fig. 4C). In these murine cases, histological examination revealed a disrupted PIE/connective tissue interface (asterisks, Fig. 4D).

Further molecular analyses at PID28 demonstrated that PIE maturation continued long after osseointegration was complete at PID14 (Fig. 2). Keratin14 expression at PID28 was equivalent to that in the JE (Fig. 4E,F). Relative to the lamellar pattern of Vimentin immunostaining in connective tissues around teeth, Vimentin was more disorganized around implants but was not noticeably different between the two surfaces (Fig. 4G,H). Visualization of picrosirius red staining under polarized light indicated that collagen around implants was less mature than collagen around teeth (Fig. 4J-L). When comparing machined vs. anodized surfaces, no significant differences in picrosirius red-stained collagen were detected (quantified in Fig. 4M). Finally, we compared Laminin5 expression in the JE (Fig. 4N,O) to its expression in the PID28 interface. Here, for the first time, Laminin5 was strongly expressed in the PIE (Fig. 4P,Q). Its expression in the PIE adjacent to a machined surface was similar to its expression in the PIE adjacent to an anodized surface (quantified in Fig. 4N).

## *Discussion*

### *The JE serves as a biomimetic blueprint for the soft tissue-implant interface*

In the past, comparisons have been made between the soft tissue-dental implant interface and the soft tissue-tooth interface e.g., the junctional epithelium (JE) (Esposito et al. 2000; Fischer and Aparicio 2022; Sculean et al. 2014; Vignoletti et al. 2009). The JE and the PIE share biological functions, in that they are intended to serve as a barrier against microbial invasion (Dhir et al. 2013; Sculean et al. 2014). The JE and PIE also may have similar attachment mechanisms e.g., via hemidesmosomes, although this is still largely unexplored in the implant space (Ayukawa et al. 2020; Shioya et al. 2009).

In this work, comparisons with the JE were used as a biomimetic blueprint of an idealized, self-renewing barrier. A number of knowledge gaps, however, act as caveats to this comparison. An intact, healthy JE was used for comparison, but the PIE is an evolving tissue that forms after an

injury e.g., tooth extraction and implant placement, and functional loading. To render a fair comparison, both tissues should be in a homeostatic state, but precisely when this is achieved in the peri-implant environment is simply unknown. It is possible the biomechanical loading influences maturation of the peri-implant soft tissues, much as it does for the JE (Yuan et al. 2023). In future experiments, we intend to compare a maturing PIE with a healing JE, say after a crown lengthening procedure, as well as the peri-implant environment around a functionally loaded implant.

### *Initial formation of the soft tissue-implant interface is equivalent around machined and anodized implants.*

We focused on dissecting the mechanisms behind formation and maturation of the soft tissue-implant interface. An immediate implant model was employed, where implants were placed in fresh extraction sockets. The reasoning behind this choice was that re-epithelialization would take longer around these implants compared to implants placed in tight-fitting osteotomies and thus would allow for a more detailed evaluation of the newly forming interface.

Integrated miniaturized murine implants were employed here, such that the abutment and body of the implant were joined and the entire surface was either machined or anodized (Fig. 1).This reliably resulted in implants with the treated surface in direct contact with soft tissues (Fig. 2). Around these implants, it was readily apparent that epithelial closure took time. For example, at PID3 the soft tissue-implant interface was a poor barrier. This conclusion was based on the lack of hemidesmosomal proteins expressed in the PIE (Fig. 3), and the fact that macrophages were abundant in the peri-implant connective tissues (Fig. 3). Nonetheless, this early timepoint allowed us to compare the peri-implant environment for any differences in peri-implant epithelial cell responses elicited by the surfaces in which they came into contact. Despite an in-depth survey, however, we found no significant molecular or cellular differences in the early interface between implants (Figs. 2,3).

### *An anodized implant surface transiently supports a better PIE attachment*

With time, however, we noted one significant change in peri-implant cell response: when we compared the relative adhesiveness of the PIE using the hemidesmosomal protein Laminin5 as a readout, we found at PID14, Laminin5 was expressed at significantly higher levels around anodized implant surfaces compared to machined surfaces (Fig. 3). At PID28, Laminin5 was increased significantly in both PIEs and there was no longer any differences between the PIEs around machined versus anodized surface (Fig. 4). Perhaps this could be attributed to lower bacterial adhesion around anodized surface abutments, reported in some recent invitro studies (Faveri et al., 2022). This transient molecular change is intriguing, but its clinical significance remains to be determined.

### *The soft tissue-implant interface matures more slowly than the hard tissue-implant interface.*

This study made clear that maturation and remodeling of a soft tissue-implant interface is a prolonged process. Long after the time when all implants had successfully osseointegrated (Fig. 2), the PIE continued to mature (Fig. 3). For purposes of comparison, the PIE matured far more slowly than the JE after a gingivectomy (Yuan et al., 2020). A similar conclusion has been reached using a rat model (Ikeda et al. 2002), and from evaluation of clinical data (Tomasi et al. 2014).

To indirectly assess barrier functions of the JE vs. PIE, the distribution of macrophages in the peri-implant and periodontal tissues was monitored. CD68 expression was gradually, significantly reduced in the peri-implant environment over time (quantified in Fig. 3P). We interpret this to mean that the attachment of the PIE is gradually improving, and analyses of Laminin5 expression support this conclusion (Fig. 4). Consequently, we urge a note of caution when assessing the barrier functions of a PIE: despite its histologic and molecular similarity to a JE, the PIE interface remodels for an extended period of time and thus its barrier functions also change over time. Any rigorous comparison of the PIEs around different types of implants should take this time-dependent maturation into account.

### *Limitations and Conclusions*

Although implants were placed in the animal model in a manner analogous to immediate implant placement in patients, a key difference is that the rodent model used extraction of healthy teeth without inflammation, whereas most patients have periodontal disease (Chrcanovic et al. 2015). This difference likely affects outcomes.

A second limitation was the variability in the expression levels of Laminin 5 and CD68 in the developing PIE (Figs. 3 and 4). Although increasing the sample size reduced this, caution is needed when interpreting attachment and inflammatory responses. Current research is addressing this variability, potentially caused by the lack of masticatory loading.

Also, it should be emphasized that tissue processing necessitated the removal of implants prior to sectioning. It is reasonable to question whether implant tissues were disturbed as a consequence. We are currently investigating embedding methods that will circumvent this technical issue while still permitting deep analyses of the molecular/cellular milieu of the soft tissue-implant interface.

Finally, it is likely that species-specific differences in mucosal integration exist, and these differences should be taken into account when considering the translational value of this work. Clinical images served to bridge this translational gap. At present, there are no molecular analyses of large animal or human peri-implant tissue responses but clearly, these are warranted to better understand the process of mucosal integration.

The nature of the soft tissue-implant interface changes dramatically over time, from a porous, single layer of epithelium to a gradually more mature epithelial barrier. Consequently, comparisons among implant surfaces, and statements about its barrier function(s), should take into account the temporal nature of its maturation. Relative to osseointegration, mucosal integration is a slow process. The prolonged timeframe of maturation and remodeling may explain why at earlier stages, the PIE is a sub-optimal barrier compared to a JE. Finally, with the analytical tools available, we found subtle biological differences in the expression of an attachment protein around machined vs. anodized abutment surfaces, the clinical significance of which remains to be determined.

## Concluding Remarks

Despite the limitations of the experiments, the culmination of the tests allow for the following conclusions. The barrier function of the PIE, as indicated by lower expression of

hemidesmosomal proteins and slower tissue maturation, appears to improve gradually over time. As corroborated by both sets of experiments, the maturation of the PIE barrier takes substantially longer than osseointegration. Given the PIE's prolonged maturation time course, strategies aimed to improve and/or accelerate PIE maturation are likely to have significant clinical benefit

*Figures and Figure legends*

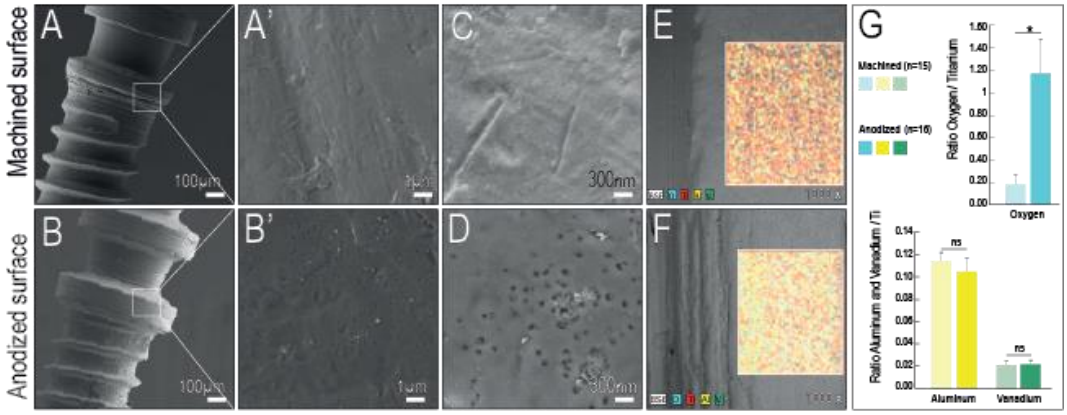


FIGURE 1

**Figure 1. Comparison analysis of machined vs. anodized implant surfaces**

Scanning electron micrograph (SEM) imaging at (A) 150x and (A') 13000x magnification of a machined titanium abutment surface, and a spark-anodized titanium oxide abutment surface shown at (B) 150x and (B') 13000x. (C) A machined titanium abutment surface and a (D) spark-anodized abutment surface, shown at 50000x to illustrate surface roughness. Energy-dispersive X-ray spectroscopy (EDX) mapping of a representative (E) machined titanium abutment and (F) spark-anodized titanium oxide abutment surface. (G) Bar graphs showing the ratio of oxygen, aluminum, vanadium to titanium of abutment surface composition. Scale bars: as indicated. Abbreviations: ns, no significance. Significance was attained at $P < 0.05$ (*), $P < 0.01$(**), and $P < 0.001$ (***).

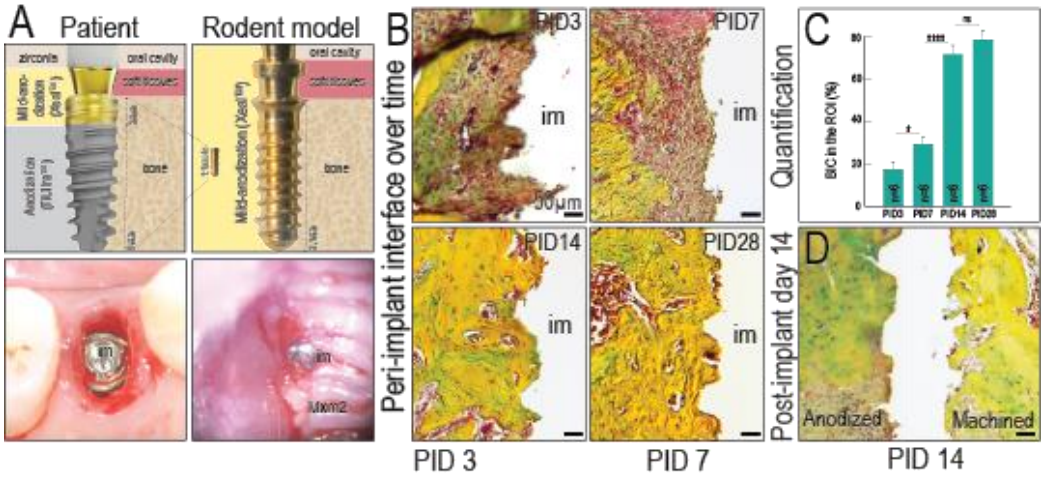


FIGURE 2

**Figure 2. Development and maturation of the soft tissue-implant interface**

(A) Schematic representation of the implant placed on a patient and an and the miniaturized version of dental implants used on our rodent model highlighting the tissues involved as well as the material distribution. Intraoral photograph of an immediate implant in a fresh extraction socket of a patient and a mouse. (B) Movat's pentachrome-stained sagittal sections of the peri-implant epithelium on multiple time points. (C) Quantification of bone implant contact (BIC) and Movat's pentachrome-stained sagittal sections on PID 14 comparing (D) an implant with machined abutment surface and an implant with an anodized abutment surface. Scale bars: as indicated. Abbreviations: mxM2, maxillary second molar; im, implant; ct, connective tissue; pie, peri-implant epithelium; e, enamel.

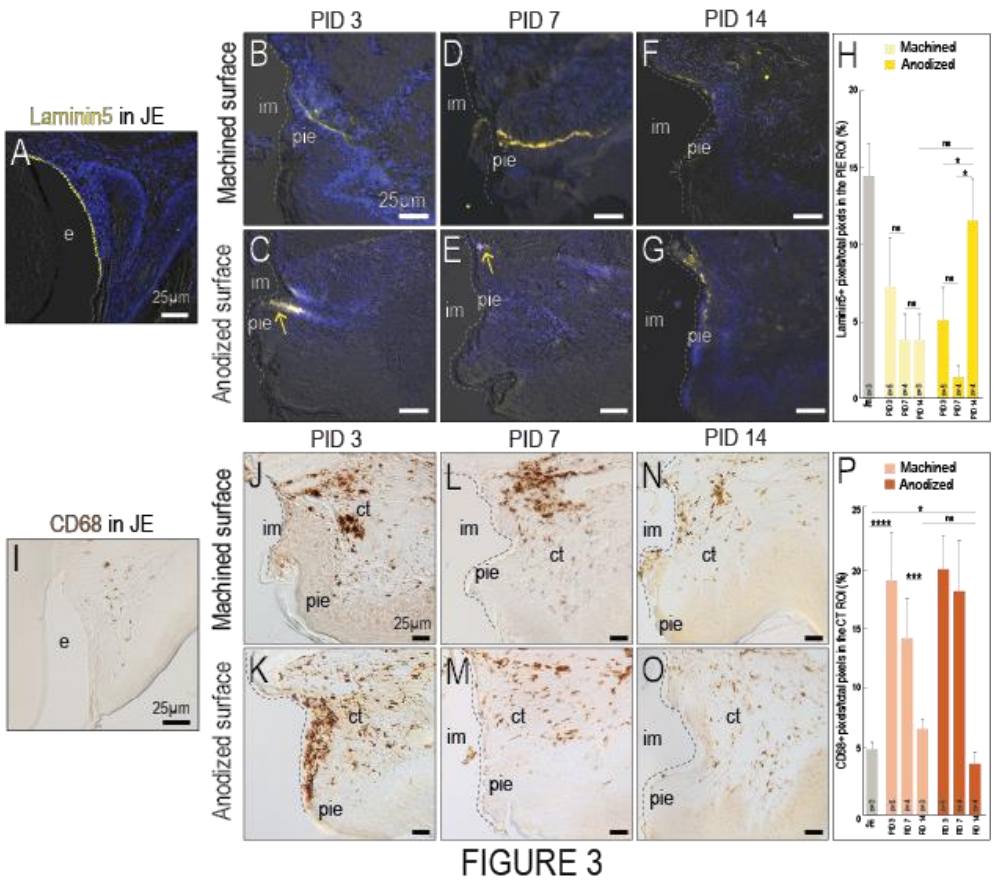


**Figure 3. Expression patterns of attachment and inflammation markers evolve during tissue maturation and are comparable between machined/anodized abutment surfaces**

Sagittal sections stained with Laminin 5 identifying hemidesmosomal attachment in: (A) a JE of a mxM1 serving as the control. In all relevant panels, the soft tissue-implant interface is delineated with the dotted line. Comparison of Laminin 5 expression in the PIE surrounding implants with machined surfaces and anodized abutment surfaces on (B,C) PID3, (D,E) PID7 and (F,G) on PID14. Quantified on (H). Sagittal sections stained with CD68 identifying macrophage activity in: (I) a JE of a mxM1 serving as the control. Comparison of CD68 expression in the PIE surrounding implants with machined abutment surfaces and anodized abutment surfaces on (J,K) PID3, (L,M) PID7 and (N,O) PID14, quantified in (P). Scale bars: as indicated. Abbreviations: as indicated in previous figures; bm, basal membrane; pie, peri-implant epithelium; ns, no significance. Significance was attained at $P < 0.05$ (*), $P < 0.01$(**), and $P < 0.001$ (***).

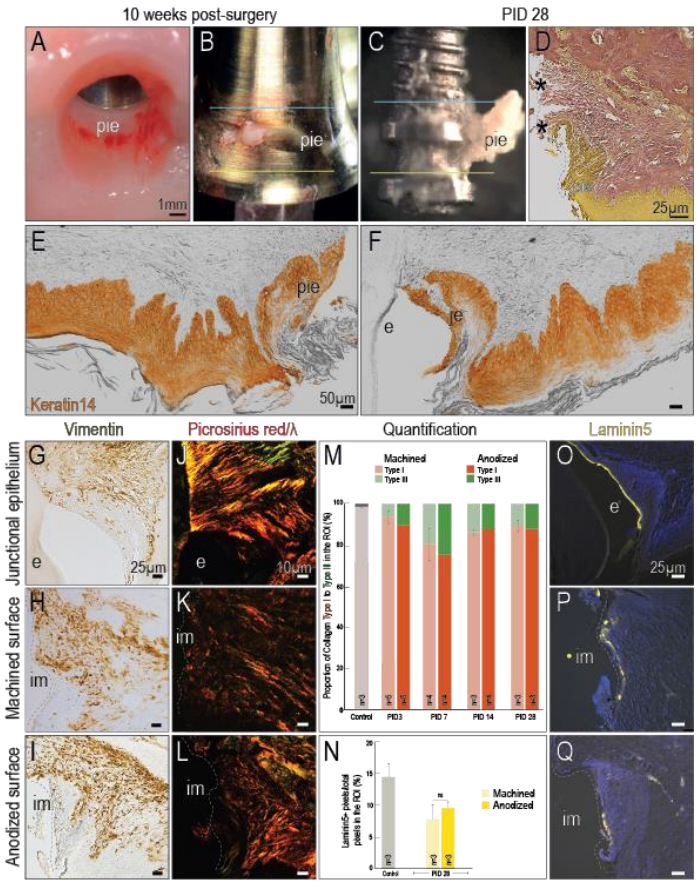


FIGURE 4

**Figure 4. Attachment proteins are upregulated in the mature PIE around both machined and anodized titanium abutment surfaces**

(A) Intraoral photograph of PIE in a patient after removal of the healing abutment, shown in (B), 10 weeks after implant placement. In all relevant panels, the soft tissue-implant interface is delineated with the dotted line. Compared to (C), a murine implant removed on PID28 and (D) Weigert's stain of the murine PIE, the asterisks indicate disruption of the tissue. Keratin 14 immunohistochemistry on PID28 of (E) PIE and (F) JE around a mxM1. Comparison of the intact JE surrounding a maxillary molar and PIE surrounding implants with machined surfaces and anodized surfaces. (G,H,I) Samples stained with Vimentin and (J,K,L) Picrosirius Red. (M) Quantification of Collagen Type I and Type III in Picrosirius Red samples in intact JE and PID3,7,14, and 28. (N) Quantification of Laminin5+ expression in intact JE and the PIE on PID28. (O,P,Q) Quantification of Laminin5 expression in intact JE, machined and anodized abutment surfaces. Scale bars: as indicated. Abbreviations: as indicated in previous figures. Significance was attained at $P < 0.05$ (*), $P < 0.01$(**), and $P < 0.001$ (***).

## References

Abrahamsson, I., Berglundh, T., & Lindhe, J. (1997). The mucosal barrier following abutment dis/reconnection. An experimental study in dogs. *J Clin Periodontol, 24*(8), 568-572. doi:10.1111/j.1600-051x.1997.tb00230.x

Aellos F, Grauer JA, Harder KG, Dworan JS, Fabbri G, Cuevas PL, Yuan X, Liu B, Brunski JB, Helms JA. 2024. Dynamic analyses of a soft tissue-implant interface: Biological responses to immediate versus delayed dental implants. J Clin Periodontol.

Arcos D, Vallet-Regi M. 2020. Substituted hydroxyapatite coatings of bone implants. J Mater Chem B. 8(9):1781-1800.

Atallah, R., Leijendekkers, R. A., Hoogeboom, T. J., & Frolke, J. P. (2018). Complications of bone-anchored prostheses for individuals with an extremity amputation: A systematic review. *PLoS ONE, 13*(8), e0201821. doi:10.1371/journal.pone.0201821

Ayukawa Y, Atsuta I, Moriyama Y, Jinno Y, Koyano K. 2020. Localization of integrin beta-4 subunit at soft tissue-titanium or zirconia interface. J Clin Med. 9(10).

Badillo-Perona, V., Cano-Sanchez, J., Campo-Trapero, J., & Bascones-Martinez, A. (2011). Peri-implant bone mechanobiology. Review of the literature. *Med Oral Patol Oral Cir Bucal, 16*(5), e677-681. doi:10.4317/medoral.17053

Bahat, O., Yin, X., Holst, S., Zabalegui, I., Berroeta, E., Perez, J., . . . Helms, J. A. (2022). An Osteotomy Tool That Preserves Bone Viability: Evaluation in Preclinical and Clinical Settings. J Clin Med, 11(9). doi:10.3390/jcm11092536

Baus-Dominguez M, Oliva-Ferrusola E, Maza-Solano S, Ruiz-de-Leon G, Serrera-Figallo MA, Gutierrez-Perez JL, Torres-Lagares D, Macias-Garcia L. 2024. Biological response of the peri-implant mucosa to different definitive implant rehabilitation materials. Polymers (Basel). 16(11).

Berglundh, T., Abrahamsson, I., Welander, M., Lang, N. P., & Lindhe, J. (2007). Morphogenesis of the peri-implant mucosa: an experimental study in dogs. *Clin Oral Implants Res, 18*(1), 1-8. doi:10.1111/j.1600-0501.2006.01380.x

Berglundh, T., Lindhe, J., Ericsson, I., Marinello, C. P., Liljenberg, B., & Thomsen, P. (1991). The soft tissue barrier at implants and teeth. *Clin Oral Implants Res, 2*(2), 81-90. doi:10.1034/j.1600-0501.1991.020206.x

Bienz SP, Hilbe M, Husler J, Thoma DS, Hammerle CHF, Jung RE. 2021. Clinical and histological comparison of the soft tissue morphology between zirconia and titanium dental implants under healthy and experimental mucositis conditions-a randomized controlled clinical trial. J Clin Periodontol. 48(5):721-733.

Blanc-Sylvestre, N., Bouchard, P., Chaussain, C., & Bardet, C. (2021). Pre-Clinical Models in Implant Dentistry: Past, Present, Future. *Biomedicines, 9*(11). doi:10.3390/biomedicines9111538

Byrd, K. M., Piehl, N. C., Patel, J. H., Huh, W. J., Sequeira, I., Lough, K. J., . . . Williams, S. E. (2019). Heterogeneity within Stratified Epithelial Stem Cell Populations Maintains the Oral Mucosa in Response to Physiological Stress. *Cell Stem Cell, 25*(6), 814-829 e816. doi:10.1016/j.stem.2019.11.005

Chrcanovic BR, Martins MD, Wennerberg A. 2015. Immediate placement of implants into infected sites: A systematic review. Clin Implant Dent Relat Res. 17 Suppl 1:e1-e16.

Coyac BR, Leahy B, Li Z, Salvi G, Yin X, Brunski JB, Helms JA. 2020. Bone formation around unstable implants is enhanced by a wnt protein therapeutic in a preclinical in vivo model. Clin Oral Implants Res. 31(11):1125-1137.

Coyac BR, Leahy B, Salvi G, Hoffmann W, Brunski JB, Helms JA. 2019. A preclinical model links osseo-densification due to misfit and osseo-destruction due to stress/strain. Clin Oral Implants Res. 30(12):1238-1249.

Dhir S, Mahesh L, Kurtzman GM, Vandana KL. 2013. Peri-implant and periodontal tissues: A review of differences and similarities. Compend Contin Educ Dent. 34(7):e69-75.

Esposito M, Thomsen P, Ericson LE, Sennerby L, Lekholm U. 2000. Histopathologic observations on late oral implant failures. Clin Implant Dent Relat Res. 2(1):18-32.

Fabbri, G., & Sorrentino, R. (2021). A Biologically Driven Concept to Design the Emergence Profile Around Dental Implants: Surgical and Prosthetic Considerations to Optimize Hard and Soft Tissue Integration. Int J Periodontics Restorative Dent, 41(6), 913-921. doi:10.11607/prd.5063

Fabbri, G., Staas, T., & Urban, I. (2022). A Retrospective Observational Study Assessing the Clinical Outcomes of a Novel Implant System with Low-Speed Site Preparation Protocol and Tri-Oval Implant Geometry. J Clin Med, 11(16). doi:10.3390/jcm11164859

Faveri, M., Lamunier, L., de Figueiredo, L. C., Meza-Mauricio, J., Scombatti de Souza, S. L., & Bueno-Silva, B. (2022). In vitro antimicrobial effect of titanium anodization on complex multispecies subgingival biofilm. *Biofouling*, *38*(6), 656–662. https://doi-org.uml.idm.oclc.org/10.1080/08927014.2022.2070431

Ferraris S, Spriano S. 2016. Antibacterial titanium surfaces for medical implants. Mater Sci Eng C Mater Biol Appl. 61:965-978.

Fischer NG, Aparicio C. 2022. Junctional epithelium and hemidesmosomes: Tape and rivets for solving the "percutaneous device dilemma" in dental and other permanent implants. Bioact Mater. 18:178-198.

Gallucci, G. O., Hamilton, A., Zhou, W., Buser, D., & Chen, S. (2018). Implant placement and loading protocols in partially edentulous patients: A systematic review. Clin Oral Implants Res, 29 Suppl 16, 106-134. doi:10.1111/clr.13276

Hall, C. W. (1974). Developing a permanently attached artificial limb. *Bull Prosthet Res*, 144-157.

Hammerle, C. H., Giannobile, W. V., & Working Group 1 of the European Workshop on, P. (2014). Biology of soft tissue wound healing and regeneration--consensus report of

Group 1 of the 10th European Workshop on Periodontology. *J Clin Periodontol, 41 Suppl 15*, S1-5. doi:10.1111/jcpe.12221

Ikeda H, Shiraiwa M, Yamaza T, Yoshinari M, Kido MA, Ayukawa Y, Inoue T, Koyano K, Tanaka T. 2002. Difference in penetration of horseradish peroxidase tracer as a foreign substance into the peri-implant or junctional epithelium of rat gingivae. Clin Oral Implants Res. 13(3):243-251.

Imber, J. C., Roccuzzo, A., Stahli, A., Bosshardt, D. D., Munoz, F., Ramseier, C. A., . . . Sculean, A. (2023). Spontaneous regeneration of keratinized tissue at implants and teeth. *J Clin Periodontol, 50*(8), 1064-1074. doi:10.1111/jcpe.13820

Iorio, V., Troughton, L. D., & Hamill, K. J. (2015). Laminins: Roles and Utility in Wound Repair. *Adv Wound Care (New Rochelle), 4*(4), 250-263. doi:10.1089/wound.2014.0533

Ivanovski, S., & Lee, R. (2018). Comparison of peri-implant and periodontal marginal soft tissues in health and disease. *Periodontol 2000, 76*(1), 116-130. doi:10.1111/prd.12150

Javed F, Vohra F, Zafar S, Almas K. 2014. Significance of osteogenic surface coatings on implants to enhance osseointegration under osteoporotic-like conditions. Implant Dent. 23(6):679-686.

Kawahara, H., Kawahara, D., Mimura, Y., Takashima, Y., & Ong, J. L. (1998). Morphologic studies on the biologic seal of titanium dental implants. Report II. In vivo study on the defending mechanism of epithelial adhesions/attachment against invasive factors. *Int J Oral Maxillofac Implants, 13*(4), 465-473.

Kulkarni, P. G., Paudel, N., Magar, S., Santilli, M. F., Kashyap, S., Baranwal, A. K., . . . Singh, A. V. (2023). Overcoming Challenges and Innovations in Orthopedic Prosthesis Design: An Interdisciplinary Perspective. *Biomed Mater Devices*, 1-12. doi:10.1007/s44174-023-00087-8

Li, Y., & Fellander-Tsai, L. (2021). The bone anchored prostheses for amputees - Historical development, current status, and future aspects. *Biomaterials, 273*, 120836. doi:10.1016/j.biomaterials.2021.120836

Lopez De Padilla, C. M., Coenen, M. J., Tovar, A., De la Vega, R. E., Evans, C. H., & Muller, S. A. (2021). Picrosirius Red Staining: Revisiting Its Application to the Qualitative and Quantitative Assessment of Collagen Type I and Type III in Tendon. J Histochem Cytochem, 69(10), 633-643. doi:10.1369/00221554211046777

Lu, E. M., Hobbs, C., Dyer, C., Ghuman, M., & Hughes, F. J. (2020). Differential regulation of epithelial growth by gingival and periodontal fibroblasts in vitro. *J Periodontal Res, 55*(6), 859-867. doi:10.1111/jre.12778

Martins-Green, M. (2013). The Yin and Yang of Integrin Function in Re-Epithelialization During Wound Healing. *Adv Wound Care (New Rochelle), 2*(3), 75-80. doi:10.1089/wound.2011.0342

Meier D, Astasov-Frauenhoffer M, Waltimo T, Zaugg LK, Rohr N, Zitzmann NU. 2023. Biofilm formation on metal alloys and coatings, zirconia, and hydroxyapatite as implant materials in vivo. Clin Oral Implants Res.

Montero, J. (2021). A Review of the Major Prosthetic Factors Influencing the Prognosis of Implant Prosthodontics. *J Clin Med, 10*(4). doi:10.3390/jcm10040816

Novaes, A. B., Kon, S., Ruben, M. P., & Goldman, H. M. (1969). Visualization of the microvascularization of the healing periodontal wound. 3. Gingivectomy. *J Periodontol, 40*(6), 359-371. doi:10.1902/jop.1969.40.6.359

Overmann, A. L., Aparicio, C., Richards, J. T., Mutreja, I., Fischer, N. G., Wade, S. M., . . . Dey, D. (2020). Orthopaedic osseointegration: Implantology and future directions. *J Orthop Res, 38*(7), 1445-1454. doi:10.1002/jor.24576

Palombo, D., Rahmati, M., Vignoletti, F., Sanz-Esporrin, J., Haugen, H. J., & Sanz, M. (2021). Hard and soft tissue healing around implants with a modified implant neck configuration: An experimental in vivo preclinical investigation. *Clin Oral Implants Res, 32*(9), 1127-1141. doi:10.1111/clr.13812

Qiao Y, Zhang W, Tian P, Meng F, Zhu H, Jiang X, Liu X, Chu PK. 2014. Stimulation of bone growth following zinc incorporation into biomaterials. Biomaterials. 35(25):6882-6897.

Ramanauskaite, A., Schwarz, F., & Sader, R. (2022). Influence of width of keratinized tissue on the prevalence of peri-implant diseases: A systematic review and meta-analysis. *Clin Oral Implants Res, 33 Suppl 23*, 8-31. doi:10.1111/clr.13766

Rocci A, Martignoni M, Burgos PM, Gottlow J, Sennerby L. Histology of retrieved immediately and early loaded oxidized implants: light microscopic observations after 5 to 9 months of loading in the posterior mandible. Clin Implant Dent Relat Res. 2003;5 Suppl 1:88-98. doi: 10.1111/j.1708-8208.2003.tb00020.x. PMID: 12691655.

Schmidlin PR, Muller P, Attin T, Wieland M, Hofer D, Guggenheim B. 2013. Polyspecies biofilm formation on implant surfaces with different surface characteristics. J Appl Oral Sci. 21(1):48-55.

Sculean, A., Gruber, R., & Bosshardt, D. D. (2014). Soft tissue wound healing around teeth and dental implants. *J Clin Periodontol, 41 Suppl 15*, S6-22. doi:10.1111/jcpe.12206

Shimono, M., Ishikawa, T., Ishikawa, H., Matsuzaki, H., Hashimoto, S., Muramatsu, T., . . . Inoue, T. (2003). Regulatory mechanisms of periodontal regeneration. *Microsc Res Tech, 60*(5), 491-502. doi:10.1002/jemt.10290

Shioya K, Sawada T, Miake Y, Inoue S, Yanagisawa T. 2009. Ultrastructural study of tissues surrounding replanted teeth and dental implants. Clin Oral Implants Res. 20(3):299-305.

Singh, D., Rai, V., & Agrawal, D. K. (2023). Regulation of Collagen I and Collagen III in Tissue Injury and Regeneration. *Cardiol Cardiovasc Med, 7*(1), 5-16. doi:10.26502/fccm.92920302

Sugawara S, Maeno M, Lee C, Nagai S, Kim DM, Da Silva J, Nagai M, Kondo H. 2016. Establishment of epithelial attachment on titanium surface coated with platelet activating peptide. PLoS One. 11(10):e0164693.

Tanaka, K., Tanaka, J., Aizawa, R., Kato-Tanaka, M., Ueno, H., Mishima, K., & Yamamoto, M. (2021). Structure of junctional epithelium is maintained by cell populations supplied from multiple stem cells. *Sci Rep, 11*(1), 18860. doi:10.1038/s41598-021-98398-7

Tian Y, Sadowsky SJ, Brunski JB, Yuan X, Helms JA. 2022. Effects of masticatory loading on bone remodeling around teeth vs. Implants: Insights from a preclinical model. Clin Oral Implants Res.

Tomasi, C., Tessarolo, F., Caola, I., Wennstrom, J., Nollo, G., & Berglundh, T. (2014). Morphogenesis of peri-implant mucosa revisited: an experimental study in humans. *Clin Oral Implants Res, 25*(9), 997-1003. doi:10.1111/clr.12223

Vignoletti F, de Sanctis M, Berglundh T, Abrahamsson I, Sanz M. 2009. Early healing of implants placed into fresh extraction sockets: An experimental study in the beagle dog. Iii: Soft tissue findings. J Clin Periodontol. 36(12):1059-1066.

Waerhaug, J. (1978). Healing of the dento-epithelial junction following subgingival plaque control. I. As observed in human biopsy material. *J Periodontol, 49*(1), 1-8. doi:10.1902/jop.1978.49.1.1

Wennerberg A, Albrektsson T, Chrcanovic B. 2018. Long-term clinical outcome of implants with different surface modifications. European journal of oral implantology. 11 Suppl 1:S123-S136.

Yuan, X., Chen, J., Gauer, J., Xu, Q., Van Brunt, L. A., & Helms, J. A. (2020). The Junctional Epithelium Is Maintained by a Stem Cell Population. *J Dent Res*, 22034520960125. doi:10.1177/0022034520960125

Yuan, X., Chen, J., Van Brunt, L. A., Grauer, J., Xu, Q., Pei, X., . . . Helms, J. A. (2020). Formation and regeneration of a Wnt-responsive junctional epithelium. *J Clin Periodontol*. doi:10.1111/jcpe.13371

Yuan, X., Liu, B., Cuevas, P., Brunski, J., Aellos, F., Petersen, J., . . . Helms, J. A. (2023). Linking the Mechanics of Chewing to Biology of the Junctional Epithelium. *J Dent Res*, 220345231185288. doi:10.1177/00220345231185288

Yuan, X., Pei, X., Chen, J., Zhao, Y., Brunski, J. B., & Helms, J. A. (2021a). Comparative analyses of the soft tissue interfaces around teeth and implants: Insights from a pre-clinical implant model. *J Clin Periodontol, 48*(5), 745-753. doi:10.1111/jcpe.13446

Yuan, X., Pei, X., Chen, J., Zhao, Y., Brunski, J. B., & Helms, J. A. (2021b). Comparative analyses of the soft tissue interfaces around teeth and implants: insights from a preclinical implant model. *Journal of Clinical Periodontology, In press.*

Yuan, X., Pei, X., Zhao, Y., Tulu, U. S., Liu, B., & Helms, J. A. (2018). A Wnt-Responsive PDL Population Effectuates Extraction Socket Healing. J Dent Res, 22034518755719. doi:10.1177/0022034518755719

Yuan, X., Pei, X., Zhao, Y., Li, Z., Chen, C. H., Tulu, U. S., . . . Helms, J. A. (2018). Biomechanics of Immediate Postextraction Implant Osseointegration. *J Dent Res*, 22034518765757. doi:10.1177/0022034518765757

Yuan, X., Xu, Q., Zhang, X., Van Brunt, L. A., Ticha, P., & Helms, J. A. (2019). Wnt-Responsive Stem Cell Fates in the Oral Mucosa. *iScience, 21*, 84-94. doi:10.1016/j.isci.2019.10.016

Zitzmann NU, Abrahamsson I, Berglundh T, Lindhe J. 2002. Soft tissue reactions to plaque formation at implant abutments with different surface topography. An experimental study in dogs. J Clin Periodontol. 29(5):456-461.

## Sample Distribution

*Table 1. Sample Distribution for Part I: Dynamic analyses of a soft tissue–implant interface: Biological responses to immediate versus delayed dental implants*

| Experiment | Timepoints | Number of Animals | Strain | Sex | Analyses |
|---|---|---|---|---|---|
| Group 1 – Immediate Implant | PID 3 | 6 | *Axin2*$^{LacZ/+}$ | M | Movat's Pentachrome<br>Masson's Trichrome<br>Aniline Blue<br>Picrosirus Red<br>Laminin 5<br>Integrin β4<br>Plectin<br>Periostin<br>CD68<br>PCNA<br>Vimentin |
| | | | *Axin2*$^{+/+}$ | F | |
| | | | *Axin2*$^{+/+}$ | M | |
| | | | *Axin2*$^{LacZ/+}$ | M | |
| | | | *Axin2*$^{LacZ/+}$ | F | |
| | | | *Axin2*$^{+/+}$ | F | |
| | PID 7 | 4 | *Axin2*$^{LacZ/+}$ | M | |
| | | | *Axin2*$^{LacZ/+}$ | F | |
| | | | *Axin2*$^{LacZ/+}$ | F | |
| | | | *Axin2*$^{LacZ/+}$ | M | |

| | | | | | |
|---|---|---|---|---|---|
| | PID 14 | 4 | *Axin2*$^{LacZ/+}$ | F | |
| | | | *Axin2*$^{+/+}$ | M | |
| | | | *Axin2*$^{LacZ/+}$ | M | |
| | | | *Axin2*$^{LacZ/+}$ | M | |
| | PID 28 | 5 | *Axin2*$^{+/+}$ | F | Movat's Pentachrome<br>Laminin 5<br>Integrin β4<br>Plectin<br>CD68<br>PCNA |
| | | | *Axin2*$^{LacZ/+}$ | F | |
| | | | *Axin2*$^{LacZ/+}$ | M | |
| | | | *Axin2*$^{LacZ/+}$ | F | |
| | | | *Axin2*$^{LacZ/+}$ | M | |
| | Total | 19 | | | |
| **Group 2 – Delayed implant** | PID 14 | 2 | *Axin2*$^{+/+}$ | M | Masson's Trichrome<br>Picrosirus Red<br>Laminin 5<br>Integrin β4<br>Plectin<br>PCNA<br>Vimentin |
| | | | *Axin2*$^{+/+}$ | F | |
| | PID 28 | 2 | *Axin2*$^{+/+}$ | F | |
| | | | *Axin2*$^{+/+}$ | M | |
| | Total | 4 | | | |
| **Ggroup 3 – MxM1 Extraction** | PED1 | 2 | *Axin2*$^{+/+}$ | F | Masson's Trichrome |
| | | | *Axin2*$^{+/+}$ | M | |
| | PED3 | 2 | *Axin2*$^{+/+}$ | F | |
| | | | *Axin2*$^{+/+}$ | F | |
| | PED 7 | 2 | *Axin2*$^{+/+}$ | F | |
| | | | *Axin2*$^{+/+}$ | F | |
| | PED 14 | 2 | *Axin2*$^{+/+}$ | M | Movat's Pentachrome<br>Masson's Trichrome |
| | | | *Axin2*$^{+/+}$ | F | |

| | | | | | |
|---|---|---|---|---|---|
| | Total | 8 | | | |
| Group 4 – Control | Intact JE | 3 | *Axin2*$^{+/+}$ | F | Movat's Pentachrome |
| | | | *Axin2*$^{+/+}$ | M | Picrosirus Red |
| | | | *Axin2*$^{+/+}$ | M | Laminin 5 |
| | | | | | Integrin β4 |
| | | | | | Plectin |
| | | | | | CD68 |
| | | | | | PCNA |
| | | | | | Vimentin |

*Table 2. Sample distribution for Part II: Dynamics of mucosal integration of machined vs. anodized titanium implants*

| Group | Timepoints | Number of implants | Strain | Sex | Analyses |
|---|---|---|---|---|---|
| Group 1 - Machined implant surface | **PID 3** | 5 | *Axin2*$^{LacZ+/+}$ | male | Movat's Pentachrome, Picrosirius Red, Laminin5, Vimentin, Keratin14 |
| | | | *Axin2*$^{LacZ+/-}$ | female | |
| | | | *Bactin*$^{GFP/+}$ | male | |
| | | | *Axin2*$^{LacZ+/+}$ | female | |
| | | | *Axin2*$^{LacZ+/-}$ | male | |
| | **PID 7** | 4 | *Axin2*$^{LacZ+/-}$ | male | |
| | | | *Axin2*$^{LacZ+/-}$ | male | |
| | | | *Axin2*$^{LacZ+/-}$ | male | |
| | | | *Axin2*$^{LacZ+/-}$ | female | |
| | **PID 14** | 3 | *Axin2*$^{LacZ+/-}$ | male | |
| | | | *Bactin*$^{GFP/+}$ | male | |
| | | | *Axin2*$^{LacZ+/-}$ | female | |
| | **PID 28** | 3 | *Axin2*$^{LacZ+/-}$ | male | Movat's Pentachrome, Picrosirius Red, Laminin5, Weigert's, Vimentin, Keratin14 |
| | | | *Axin2*$^{LacZ+/-}$ | male | |
| | | | *Axin2*$^{LacZ+/-}$ | female | |

| | | | | | |
|---|---|---|---|---|---|
| Group 2 - Anodized implant surface | **PID 3** | 5 | *Axin2*$^{LacZ\ +/+}$ | male | Movat's Pentachrome, Picrosirius Red, Laminin5, CD68, Keratin14 |
| | | | *Axin2*$^{LacZ\ +/-}$ | female | |
| | | | *Bactin*$^{GFP/+}$ | male | |
| | | | *Axin2*$^{LacZ+/+}$ | female | |
| | | | *Axin2*$^{LacZ+/-}$ | male | |
| | **PID 7** | 4 | *Axin2*$^{LacZ\ +/-}$ | male | |
| | | | *Axin2*$^{LacZ\ +/-}$ | male | |
| | | | *Axin2*$^{LacZ\ +/-}$ | male | |
| | | | *Axin2*$^{LacZ\ +/-}$ | female | |
| | **PID 14** | 4 | *Axin2*$^{LacZ\ +/-}$ | male | |
| | | | *Bactin*$^{GFP/+}$ | male | |
| | | | *Axin2*$^{LacZ\ +/-}$ | female | |
| | | | *Axin2*$^{LacZ\ +/-}$ | male | |
| | **PID 28** | 3 | *Axin2*$^{LacZ\ +/-}$ | male | Movat's Pentachrome, Picrosirius Red, Laminin5, Weigert's, Vimentin, Keratin14 |
| | | | *Axin2*$^{LacZ\ +/-}$ | male | |
| | | | *Axin2*$^{LacZ\ +/-}$ | female | |

| Control Group | Timepoints | Number of Animals | Strain | Sex | Analyses |
|---|---|---|---|---|---|
| Intact MxM1 | **Intact** | 3 | *Axin2*$^{LacZ+/+}$ | male | Movat's Pentachrome, Picrosirius Red, Laminin5, Weigert's, CD68, Vimentin, Keratin14 |
| | | | *Axin2*$^{LacZ+/+}$ | male | |
| | | | *Axin2*$^{LacZ+/+}$ | female | |

# Appendix

## *Part I Appendix Data*

### *Tissue processing*

Immediately upon harvest, murine tissues were washed in ice-cold phosphate buffered saline (PBS) followed by fixation in 4% paraformaldehyde (PFA) for 24h at 4°C. All tissues were then rinsed in PBS and decalcified in 10% EDTA in a microwave (Ted Pella, CA, USA) at 25°C for ~2 weeks. Thereafter tissues were dehydrated by a graded ethanol series, embedded in paraffin, and sectioned into 8µm thin slides using a Leica microtome (Leica Instruments, Hubloch, Germany).

### *Histology*

#### Pentachrome

Tissue sections were deparaffinized with Citrisolv for a total of 10 minutes, then rehydrated in a graded ethanol series. Slides were stained with 1% Alcian blue (#A5268, Sigma) for 20 minutes then submerged in running tap water to de-stain for 10 minutes. Thereafter, slides were stained in Verhoeff's Hematoxylin for 5 min, and submerged in running tap water to de-stain for 5 minutes. A fresh solution containing 7.85% w/v Sodium Thiosulfate (14518, Alfa Aesar, MA) was prepared and the slides treated therein for 1 minute, followed by running tap water to de-stain for 5 minutes. Slides were treated with a fresh solution containing 0.08% w/v Crocein-Scarlet (22914, Chem Impex International, IL) and 0.02% w/v 5Acid Fuchsin (22914, Chem Impex International, IL; F8129, Sigma) solution, both dissolved in 1% glacial acetic acid and ddH2O for 8 minutes, followed by de-staining via 9 dips in dd$H_2O$ followed by 10 additional dips in 0.5% acetic acid. Slides were submerged in 5% phosphotungstic acid (P4006, Sigma) for 15 minutes then de-stained in 0.5% acetic acid for 1 minute. Slides were subsequently washed in absolute ethanol for 5 minutes with three changes. Last, slides were stained in a solution containing 3% w/v Saffron (3801, Harlecon) dissolved in ethanol for 60 minutes. Thereafter, slides were dehydrated in an ascending ethanol series, followed by Citrisolv. Finally, the slides were cover-slipped using a mounting medium (Permount, SP15-100, Fisher Scientific).

#### Masson's Trichrome

Masson's trichrome staining of the slides followed the protocol provided by Electron Microscopy Sciences (EMS Catalog #26386). Tissue sections were deparaffinized with Citrisolv for a total of 10 minutes, then rehydrated in a graded ethanol series. Slides were incubated with Bouin's fixative for 1 hour at 56°C then washed with running tap water for 5 minutes. Thereafter, slides were stained with Weigert's iron hematoxylin for 5 minutes then washed with running tap water for 10 minutes. Slides were submerged in Biebrich scarlet-acid fuchsin for 12 minutes then rinsed with ddH2O. Slides were subsequently stained with phosphomolybdic acid-phosphotungstic acid for 15 minutes then rinsed with ddH2O. Slides were stained with Aniline Blue solution for 2 minutes then rinsed with ddH2O. Last, slides were differentiated in 1% acetic acid for 4 minutes. Tissue sections were then dehydrated using a graded ethanol series to Citrisolv and cover-slipped using mounting medium (Permount, SP15-100, Fisher Scientific).

**Picrosirius Red**

Tissue sections were deparaffinized with Citrisolv and a graded ethanol series, then stained in a solution of Weigert's iron hematoxylin for 8 min. Sections were washed then stained in Picrosirius red solution for 1 hour and differentiated in a solution of 1% acetic acid (Lopez De Padilla et al., 2021). Tissue sections were then dehydrated using a graded ethanol series to Citrisolv and cover-slipped using mounting medium (Permount, SP15-100, Fisher Scientific).

### *Quantitative immunohistochemistry (qIHC)*

Quantitative immunostaining followed our published protocols (Yuan et al., 2018). In brief, tissue sections were de-paraffinized then permeabilized with 0.5% TritonX-100. All slides are subjected to the identical procedure wherein antigen retrieval was performed using Antigen Unmasking Solution (Vector Labs), following which slides were blocked with 5% goat serum (Vector S-1000) for 1h at room temperature then incubated with primary antibodies overnight at 4°C. After washing with PBS, slides destined for immunofluorescence using the following antibodies e.g., Laminin5 (1:200 dilution, ab14509, Abcam), anti-CD104 (1:200; 553745, BD bioscience), Plectin (1:250, ab32528, Abcam), were incubated with Cyanine5 conjugated goat anti-rabbit secondary antibody (1:400, Invitrogen, A-10523) for 30 min, then mounted with 4',6-diamidino-2-phenylindole (DAPI) mounting medium (Vector Labs).

Primary antibodies developed with DAB peroxidase used in this study included Proliferating Cell Nuclear Antigen (PCNA; 1:2000, ab18197, Abcam), Vimentin (1:250 dilution, 5741, Cell Signaling Technology) and CD68 (1:150 dilution, MAB101141, R&D Systems). The secondary antibody used to detect these primary antibodies was biotinylated goat anti-rabbit immunoglobulin G antibody (1:200, BA-1000, Vector Laboratories). Staining was then visualized using the ABC peroxidase standard staining kit (32020, Thermo Fisher Scientific) and the DAB peroxidase substrate kit (SK4100, Vector Lab).

### *Quantification*

#### Soft tissue thickness

It was conducted on pentachrome slides taken at 20x magnification on the Leica microscope, using its DMi8 digital imaging system. Adobe Photoshop was employed to take the measurements, where the "ruler tool" (corrected for real-life distances) was employed to measure the thicknesses of connective tissue (CT), epithelium (epi) and combined thickness (CT+epi) in pixels. Total thickness was defined as the distance from epithelial surface to alveolar bone, approximately parallel to the trajectory of the long axis of the implant (perpendicular to plane of alveolar bone). A series of 10 vertical measurements (spanning ~150-200µm section of tissue) on 3 images per time point (PID 3, 7, 14, and 28), in a section slightly away from the implant-soft tissue interface were taken. The measurements were taken slightly away from the soft tissue implant interface to get sections of tissues that had a clear epithelium/connective tissue, as the tissue immediately adjacent to the implant is primarily epithelium or the transition between the two became slightly distorted.

#### Cell proliferation and macrophage activity

To quantify the expression of PCNA (cell proliferation marker) and CD68 (macrophage activity), the positive control tissue was an intact mxM1; and then compared to samples from PID 3, 7, 14 and 28. All images were taken at the same magnification, and region of interest (ROI) was selected. The ROIs for the control samples were the junctional epithelium (JE) and CT, and then compared against the ROIs in the implant samples peri-implant epithelium (PIE) and CT respectively, in the multiple timepoints. A minimum of three tissue sections were analyzed from each sample. Within the specified ROI, the total pixel area was quantified, and the total number of pixels representing positive signal e.g., PCNA+ cells, CD68+ cells was selected and quantified using Adobe Photoshop's, where selection of the ROI was performed using the "magnetic lasso" tool. Selecting positive pixels was then facilitated by the "magic wand tool" and adjusting the selected expression with the "grow" and "similar" functions, with tolerance for both these parameters set between 1-10. The area of signal-positive cells was then divided by the total pixels in the ROI.

### Attachment proteins

To quantify the hemidesmosomal attachment proteins: Laminin5, ß4 integrin, and Plectin, the positive control tissue was an intact mxM1; and then compared to samples from PID 3, 7, 14 and 28. All images were taken at the same magnification, and region of interest (ROI) was selected, the JE of an intact mxM1 was compared against the PIE (see Appendix Fig.4A,C) and the basement membrane (BM (see Appendix Fig.4B,D)) of an intact mxM1 was compared against the BM from the implant samples, in the multiple timepoints. A minimum of three tissue sections were analyzed from each sample. Within the specified ROI, the total pixel area was quantified, and the total number of pixels representing positive signal e.g., Laminin5+ expression, was selected and quantified using Adobe Photoshop's, where selection of the ROI was performed using the "magnetic lasso" tool. Selecting positive pixels was then facilitated by the "magic wand tool" and adjusting the selected expression with the "grow" and "similar" functions, with tolerance for both these parameters set between 1-10. The area of signal-positive cells was then divided by the total pixels in the ROI.

### Collagen fiber maturation

To identify and quantify the amount of collagen type I and type III using Picrosirus red stained sections, the positive control tissue was an intact mxM1; and then compared to samples from PID 3, 7, 14 and 28. All images were taken at the same magnification, and region of interest (ROI) was selected, the CT of an intact mxM1 was compared against the CT in the implant samples. A minimum of three tissue sections were analyzed from each sample. Within the specified ROI, the total pixel area was quantified, and the total number of pixels representing collagen type I (red/orange) and collagen type III (green), was selected and quantified using Adobe Photoshop's, where selection of the ROI was performed using the "magnetic lasso" tool. Selecting positive pixels was then facilitated by the "magic wand tool" and adjusting the selected expression with the "grow" and "similar" functions, with tolerance for both these parameters set between 1-10. The area of signal-positive cells was then divided by the total pixels in the ROI and a ratio of type I collagen to type III collagen was calculated.

### *Statistical analyses*

Bar charts were used to present the results as the mean ± standard deviation of independent replicates. Some sample means were measured to be very close to zero, which could lead to a right-skewed distribution, as no measurement could be negative. Due to this and the small sample sizes, it was decided that a normal distribution of the data could not be assumed. Thus, parametric tests could not be used. The non-parametric Mann-Whitney U test was used to determine whether or not sample means from two groups differed. Significance was attained at $P< 0.05$(*) and $P< 0.01$(**).

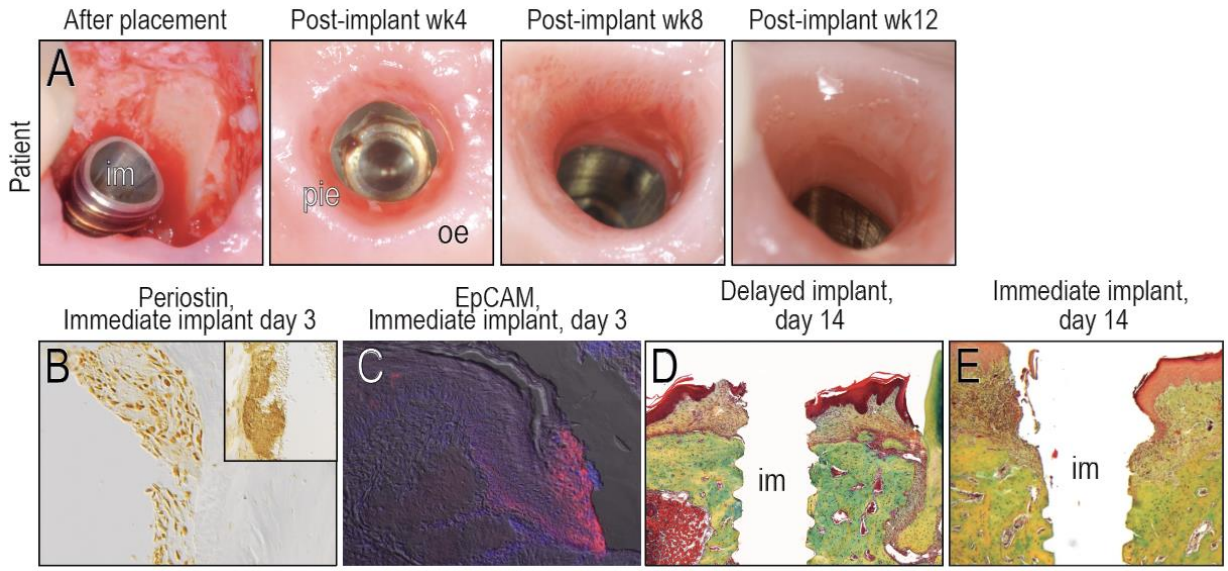


*Appendix Fig 1. Tissue contributions to the soft tissue-implant interface.*

(A) Sequence of intraoral clinical photographs of an immediate implant after placement, and on post-implant week 4, 8, and 12. In those cases from weeks 4, 8, and 12, photographs were made after removal of the healing abutment. (B) Quantitative IHC of Periostin expression in the implant bed around an immediate implant on PID14; boxed area in upper right corner illustrates remnants of the PDL ligament left behind after tooth extraction. Quantitative IHC of EpCAM expression in the epithelium around an immediate implant on PID3. (C) osseointegration of a delayed implant on post-implant day 14; and osseointegration of a (D) delayed and (E) immediate implant at the same time point.

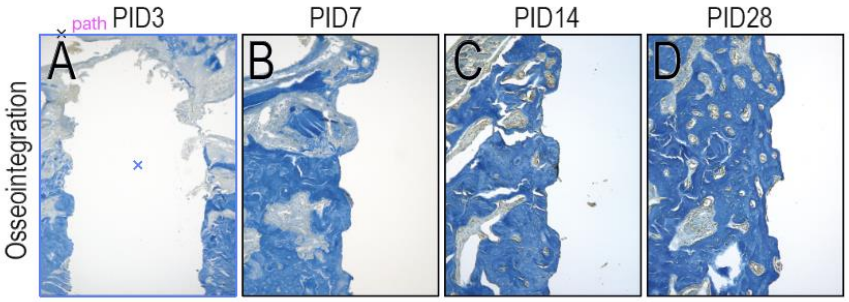

*Appendix Fig 2. Osseointegration over time in a dental implant rodent model.*

Aniline blue-stained sagittal sections representing osseointegration in a rodent model over time. Multiple time points are illustrated: (A) post-implant day (PID)3, (B) PID7, (C) PID14 and (D) PID28.

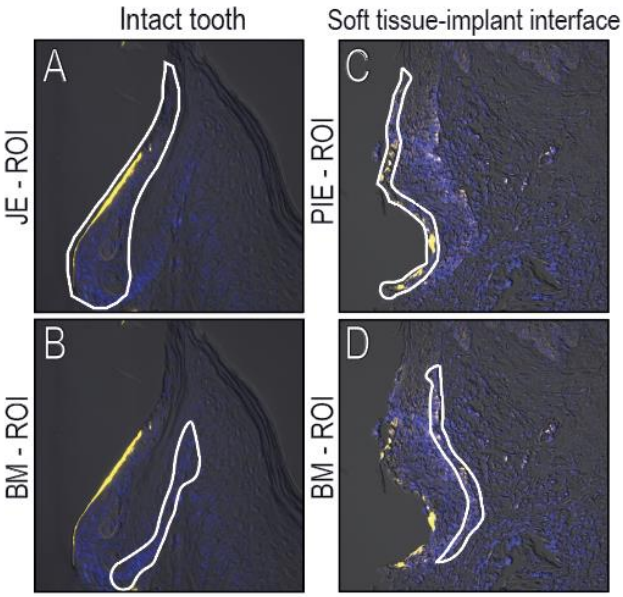


*Appendix Fig 3. Definition of ROIs for quantification.*

Slides depicting region of interests (ROIs). (A) ROI of epithelial-tooth interface of the junctional epithelium (JE) used for the attachment proteins (e.g., Laminin 5). (B) Depicting the ROI used to quantify the basement membrane (BM) around teeth for all attachment proteins. (C) Depicting the ROI used to quantify the epithelial-implant interface of the peri-implant epithelium (PIE) used for the attachment proteins (e.g., Laminin 5). (D) Depicting the ROI used to quantify the basement membrane (BM) around implants for all attachment proteins.

## *Part II: Appendix Data*

### *Mice*

Protocols were approved by the Stanford Committee on Animal Research under #13146. Sexteen 5-week-old BALB/cJ male and female mice constituted the 2 test groups (machined and anodized implant), and three 5-week-old BALB/cJ male and female mice constituted the control group, intact maxillary first molars (JE). All mice were housed in a temperature-controlled environment in a 12-hour light/dark cycle. Water and food were offered ad libitum.

### *Surgeries*

**Tooth extraction**

All procedures conformed to ARRIVE guidelines. Rodents were anesthetized with ketamine (80-100 mg/kg bodyweight) and xylazine (8 mg/kg bodyweight), administered intraperitoneally.

Analgesia was ensured by subcutaneous Buprenorphine SR (1.5 mg/kg bodyweight) injection. Bilateral maxillary first molar (mxM1) extractions were performed using micro-forceps; bleeding was controlled by local compression. Information on the strains and gender of mice can be found in Table 1.

**Implants**

One set of miniaturized implants had a machined surface (control group), manufactured of a titanium (Titanium-6 Aluminum-4 Vanadium) alloy, with 0.5mm diameter and 2.1mm length (Edenta, Switzerland). The second set of implants was coated with a titanium oxide layer via a proprietary (Nobel Biocare AB, Göteborg, Sweden) mild-anodization process (test group), resulting in an implant with a 0.62mm diameter and the same 2.1mm length. Implants used in this murine study did not have a separate abutment. Consequently, the anodized abutment surface extended along the whole structure (from the apex to the top of the implant and ensured that either a machined surface or an anodized surface was adjacent to the connective tissue and PIE at all timepoints (Fig. 2).

**Implant placement and time points for analysis**

Immediately after extraction, hemostasis was achieved, and implants were manually inserted with an implant screwdriver into the mxM1 palatal root socket. This screwdriver is specific for the miniaturized murine implants. The dimension of the palatal socket e.g., 0.274 $mm^3$, was determined by µCT analysis; this was sufficient in size to accommodate miniatured implants and ensure primary stability. All implants were placed manually, using an implant-specific screwdriver. To align with clinical data where the threaded portion of the implant was placed 2mm below the alveolar bone crest, in the animal model, the threaded portion of the implant was also placed below the alveolar bone crest. In the patient, the abutment portion of the implant was contained within the soft tissue. In the animal model, the non-threaded portion of the implant, which had either a machined or an anodized surface, projected above the soft tissue but was positioned below the occlusal plane. This projection above the soft tissue was necessary to allow for removal of the implant after the animal had been sacrificed but before tissue processing (Fig. 2). Soft tissue implant-interfaces were examined on post-implant days (PID) 3, 7, 14, and 28. There was no evidence of infection or prolonged inflammation at surgical sites, nor around implants. No antibiotics were given to operated animals.

*Patient sample*

After informed consent, a female patient, aged 37 with no history of systemic or periodontal diseases but a history of light (< 8cigarettes/day) smoking, underwent extraction of the maxillary first premolar due to a vertical root fracture. The patient received an immediate implant in combination with xenograft biomaterial on the buccal surface accompanied by a connective tissue graft harvested from the palate that was positioned using a tunneling technique. The position for the dental implant was obtained using a digital 3D prosthetic model (DTX Studio Implant). The implant body (threaded portion) was placed 2 mm below the alveolar crest (see Figure 2). To create an emergence profile, the implant had 4 mm distance from the implant platform to the gingival margin (Fabbri and Sorrentino 2021). An N1 (Nobel Biocare) implant was used utilizing a low-speed (50rpm) drilling protocol without irrigation (Bahat et al. 2022; Chen et

al. 2019; Coyac et al. 2021; Fabbri et al. 2022). The implant achieved primary stability of at least 30 Ncm. The implant was not subjected to immediate loading due to a history of bruxism.

### *Tissues*

Immediately upon harvest, tissues were washed in ice-cold phosphate buffered saline (PBS) followed by fixation in 4% paraformaldehyde (PFA) for 24h at 4°C. All tissues were then rinsed in PBS and decalcified in 10% EDTA in a microwave (Ted Pella, CA, USA) at 25°C for ~2 weeks. Thereafter tissues were dehydrated by a graded ethanol series, and the implants were carefully removed under visual control. The tissues where then embedded in paraffin and sectioned into 8µm slides using a Leica microtome (Leica Instruments, Hubloch, Germany).

### *Surface analysis by SEM*

Scanning electron microscopy (SEM) images were acquired both on a Gemini 450 (Zeiss) and on a tabletop microscope TM3000 (Hitachi). At least three different areas were scanned at 80x, 13000x and 50000x magnification, on three different samples, and representative images were chosen. Energy-dispersive X-ray spectroscopy (EDX), an analytical method for chemical characterization of the implant surface, was performed by imaging at least three different areas at 1000x magnification and 15 kV beam voltage acceleration. After acquisition, EDX maps were analyzed with Quantax 70 software (Brucker).

### *Histology*

#### Pentachrome

Tissue sections were deparaffinized with Citrisolv for a total of 10 minutes, then rehydrated in a graded ethanol series. Slides were stained with 1% Alcian blue (#A5268, Sigma) for 20 minutes then submerged in running tap water to de-stain for 10 minutes. Thereafter, slides were stained in Verhoeff's Hematoxylin for 5 min, and submerged in running tap water to de-stain for 5 minutes. A fresh solution containing 7.85% w/v Sodium Thiosulfate (14518, Alfa Aesar, MA) was prepared and the slides treated therein for 1 minute, followed by running tap water to de-stain for 5 minutes. Slides were treated with a fresh solution containing 0.08% w/v Crocein-Scarlet (22914, Chem Impex International, IL) and 0.02% w/v 5Acid Fuchsin (22914, Chem Impex International, IL; F8129, Sigma) solution, both dissolved in 1% glacial acetic acid and ddH2O for 8 minutes, followed by de-staining via 9 dips in ddH2O followed by 10 additional dips in 0.5% acetic acid. Slides were submerged in 5% phosphotungstic acid (P4006, Sigma) for 15 minutes then de-stained in 0.5% acetic acid for 1 minute. Slides were subsequently washed in absolute ethanol for 5 minutes, x3. Last, slides were stained in a solution containing 3% w/v Saffron (3801, Harlecon) dissolved in ethanol for 60 minutes. Thereafter, slides were dehydrated in an ascending ethanol series, followed by Citrisolv. Finally, the slides were cover-slipped using a mounting medium (Permount, SP15-100, Fisher Scientific).

#### Weigert's

Tissue sections were deparaffinized with Citrisolv and a graded ethanol series, then stained in a solution of Weigert's iron-hematoxylin for 10 min. Thereafter, slides were submerged in running tap water to de-stain for 10 minutes. Slides were stained in Resorcin-Fuchsin (#2637-01, Electron Microscopy Sciences) solution for 60 minutes, then submerged in running tap water to de-stain

for 1 minute. Slides were then treated with Van Giseon's (#26370-02, Electron Microscopy Sciences) solution for 30 seconds. Tissue sections were then dehydrated using a graded ethanol series to Citrisolv and cover-slipped using mounting medium (Permount, SP15-100, Fisher Scientific).

**Picrosirius Red**

Tissue sections were deparaffinized with Citrisolv and a graded ethanol series, then stained in a solution of Weigerts iron-hematoxylin for 8 min. Sections were washed then stained in Picrosirius red solution for 1 hour and differentiated in a solution of 1% acetic acid (Lopez De Padilla et al. 2021). Tissue sections were then dehydrated using a graded ethanol series to Citrisolv and cover-slipped using mounting medium (Permount, SP15-100, Fisher Scientific).

### *Quantitative immunohistochemistry (qIHC)*

Immunostaining followed published protocols (Yuan et al. 2018). In brief, tissue sections were de-paraffinized then permeabilized with 0.5% TritonX-100. Antigen retrieval was performed using Antigen Unmasking Solution (Vector Labs), following which slides were blocked with 5% goat serum (Vector S-1000) for 1h at room temperature then incubated with primary antibodies overnight at 4°C. After washing with PBS, slides destined for immunofluorescence, Laminin-5 (1:200, ab14509, Abcam), were incubated with Cyanine5 conjugated goat anti-rabbit secondary antibody (1:400, Invitrogen, A-10523) for 30 min, then mounted with 4',6-diamidino-2-phenylindole (DAPI) mounting medium (Vector Labs). Primary antibodies developed with DAB peroxidase used in this study include Keratin14 (1:200, Biolegend, 905304), Vimentin (5741, 1:250, Cell Signaling Technology) and CD68 (1:150, MAB101141, R&D Systems). The secondary antibody used to detect these primary antibodies was biotinylated goat anti-rabbit immunoglobulin G antibody (1:200, BA-1000, Vector Laboratories). Staining was then visualized using the ABC peroxidase standard staining kit (32020, Thermo Fisher Scientific) and the DAB peroxidase substrate kit (SK4100, Vector Lab).

### *Quantification*

**Laminin 5**

To quantify the hemidesmosomal attachment protein Laminin5, a standard process was employed where regions of interest (ROI) were photographed using a minimum of 1 image per sample, and 3 separate samples per timepoint. Pictures were taken at 20x magnification on the Leica microscope, using its DMi8 digital imaging system and quantified in a double-blinded manner by two independent investigators (J.G and K.H).

The positive control tissue was the JE around an intact maxillary first molar (mxM1). Quantification of this expression domain was then compared to expression of Laminin5 in soft tissue-implant interface from samples at PID3, 7, 14 and 28 around both machined and anodized implants.

The region of interest (ROI) was selected based on the morphology of the peri-implant epithelium. The region of interest (ROI) (see Appendix Fig. 3) was defined as a thin band of tissue in the region of the JE/PIE, using anatomic landmarks. Specifically, it encompassed the non-keratinized tissue of the sulcular/peri-implant epithelium, from the coronal most-aspect to the

base of the sulcus. Within the specified ROI, the total pixel area was quantified, and the total number of pixels representing positive signal e.g., Laminin5+ expression, was selected and quantified using Adobe Photoshop's, where selection of the ROI was performed using the "magnetic lasso" tool. Selecting positive pixels was then facilitated by the "magic wand tool" and adjusting the selected expression with the "grow" and "similar" functions, with tolerance for both these parameters set between 1-10. The area of signal-positive cells was then divided by the total pixels in the ROI. A minimum of three tissue sections were analyzed from each sample.

**CD68**

To quantify the expression of CD68 (macrophage activity), a standard process was employed where regions of interest (ROI) were photographed using a minimum of 1 image per sample, and 3 separate samples per timepoint. Pictures were taken at 20x magnification on the Leica microscope, using its DMi8 digital imaging system and quantified in a double-blinded manner by two independent investigators (J.G and K.H).

The positive control tissue was an intact mxM1; and then compared to samples from PID 3, 7, 14 and 28 from both machined and anodized implant surfaces. The ROI for the control samples were the connective tissue of an intact mxM1, and then compared against the ROI in the implant samples (connective tissue of the soft tissue implant interface) at multiple timepoints (see Appendix Fig. 3). Within the specified ROI, the total pixel area was quantified, and the total number of pixels representing positive signal e.g., CD68+ cells was selected and quantified using Adobe Photoshop's, where selection of the ROI was performed using the "magnetic lasso" tool. Selecting positive pixels was then facilitated by the "magic wand tool" and adjusting the selected expression with the "grow" and "similar" functions, with tolerance for both these parameters set between 1-10. The area of signal-positive cells was then divided by the total pixels in the ROI.

**Picrosirius Red**

To identify and quantify the amount of collagen type I and type III using Picrosirius red stained sections, a standard process was employed where regions of interest (ROI) were photographed using a minimum of 1 image per sample, and 3 separate samples per timepoint. Pictures were taken at 40x magnification on the Leica microscope, using its DMi8 digital imaging system and quantified in a double-blinded manner by two independent investigators (J.G and K.H).

The positive control tissue was an intact mxM1; and then compared to samples from PID 3, 7, 14 and 28. The region of interest (ROI) was selected, the CT of an intact mxM1 was compared against the CT in the implant samples (see Appendix Fig. 3). A minimum of three tissue sections were analyzed from each sample. Within the specified ROI, the total pixel area was quantified, and the total number of pixels representing collagen type I (red/orange) and collagen type III (green), was selected and quantified using Adobe Photoshop's, where selection of the ROI was performed using the "magnetic lasso" tool. Selecting positive pixels was then facilitated by the "magic wand tool" and adjusting the selected expression with the "grow" and "similar" functions, with tolerance for both these parameters set between 1-10. The area of signal-positive cells was then divided by the total pixels in the ROI and a ratio of type I collagen to type III collagen was calculated.

**Bone Implant Contact**

To quantify the bone implant contact (BIC), a standard process was employed where regions of interest (ROI) were photographed using a minimum of 1 image per sample, and 3 separate samples per timepoint. Pictures were taken at 10x magnification on the Leica microscope, using its DMi8 digital imaging system and quantified.

Samples from PID 3, 7, 14 and 28 were used. The ROI was the peri-implant bone in direct contact with the threads of the implant, at all the timepoints in addition to this, we have added representative histological images (see Fig. 2). Within the specified ROI, the total pixel area was quantified, and the total number of pixels representing the bone using Pentachrome histology images was selected and quantified using Adobe Photoshop's, where selection of the ROI was performed using the "magnetic lasso" tool. Selecting positive pixels was then facilitated by the "magic wand tool" and adjusting the selected expression with the "grow" and "similar" functions, with tolerance for both these parameters set between 1-10. The area of peri-implant bone in direct contact with the threads of the implant was then divided by the total pixels in the ROI.

### *Statistical analyses*

A minimum statistical power of 0.8 was selected to ensure the detection of significant results. Small intergroup differences were deemed insufficiently meaningful, leading to adoption a relatively large effect size of 2.5 standard deviations to avoid the use of additional animals. Consequently, a minimum of three mice per group was determined to be necessary to achieve the desired power. Some groups e.g., PID3 and PID7, contained 1-2 additional mice, resulting in an overall power range from 0.86 to 0.98. Results are presented as the mean ± standard deviation of independent replicates. Student's t-test was used to quantify differences between groups at a specific time point. An unpaired t-test was used for independent variables and paired t-test for non-independent variables. Significance was attained at $P < 0.05$ (*), $P < 0.01$(**), and $P < 0.001$ (***).

### *Appendix Figure 1: Experimental design*

Flowchart of split-mouth design of the study, sample distribution, timepoints and implants surfaces analyzed.

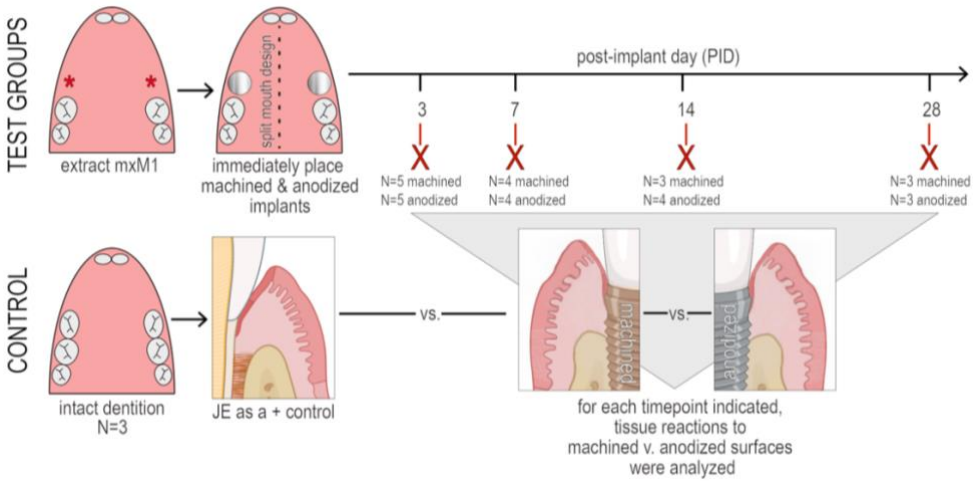

*Appendix Figure 2: Cell density in peri-implant interface.*

Cell density in the peri-implant interphase at the time were osseointegration is accomplished was analyzed (white arrows indicate cell nuclei identify in blue by DAPI). Scale bars: as indicated. Abbreviations: as indicated in previous figures.

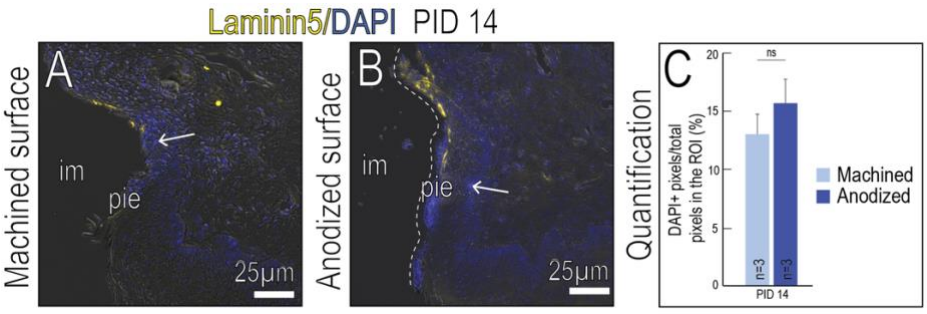


*AppendixFigure 3: Definition of ROIs for quantification.*

Slides depicting region of interests (ROIs). (A) ROI of epithelial-tooth interface of the junctional epithelium (JE) used for the attachment proteins (e.g., Laminin 5). (B) Depicting the ROI used to quantify the epithelial-implant interface of the peri-implant epithelium (PIE) used for the attachment proteins (e.g., Laminin 5). (C) ROI of the connective tissue adjacent to the JE were CD68 is expressed (D) Depicting the ROI used to quantify the expression of CD68 on the connective tissue adjacent to the PIE. (E) ROI of the connective tissue adjacent to the JE and (F) in the peri-implant interphase where collagen fibers are stained with Picrosirius red.